Wide Bandgap Semiconductors: Thin Film Properties and Luminescence Efficiency Improvement

A Thesis

Presented in Partial Fulfillment of the

Requirements for the

Degree of Master of Science

with a

Major in Physics

in the

College of Graduate Studies

University of Idaho

by

Jeffrey Lapp

Major Professor: Leah Bergman, Ph.D.

Committee Members: Ruprecht Machleidt, Ph.D.; M. Grant Norton, Ph.D.

Department Administrator: John Hiller, Ph.D.

May 2020

Authorization to Submit Thesis

This thesis of Jeffrey Lapp, submitted for the degree of Master of Science with a Major in Physics and titled "Wide Bandgap Semiconductors: Thin Film Properties and Luminescence Efficiency Improvement" has been reviewed in final form. Permission, as indicated by the signatures and dates below, is now granted to submit final copies to the College of Graduate Studies for approval.

Major Professor: _____ Date: _____
Leah Bergman, Ph.D.

Committee Members: _____ Date: _____
Ruprecht Machleidt, Ph.D.

_____ Date: _____
M. Grant Norton, Ph.D.

Department Administrator: _____ Date: _____
John Hiller, Ph.D.

Abstract

Modern technological applications require high performance materials that possess novel properties to efficiently operate in a wide range of conditions. In this work, the performance enhancement of ZnO thin films was studied, while basic research on the optical properties of Ga_2O_3 thin films was performed.

Two approaches for the enhancement of the UV band edge photoluminescence (PL) in sputtered ZnO films were studied. One that used surface coating, and another that employed annealing in a non-oxidizing environment. It was found that by combining both methods, annealing at an optimal temperature followed by the deposition of a coating, a significant enhancement of the luminescence can be achieved. Three types of coatings were investigated, Al_2O_3, SiO_2, and MgO. It was found that MgO, due to its strong bond energy, is an effective coating material for the passivation of the surfaces of the ZnO films. The UV-PL intensity of MgO coated ZnO was found to increase by a factor of ~ 52 relative to an uncoated film. The effectiveness of the coating layer was discussed in terms of competing mechanisms to surface passivation, such as the adsorption of OH-groups, which can act as surface traps and diminish PL intensity. Moreover, annealing at 900° C prior to the deposition of the coating was found to be an important step in realizing the optimal performance of the coating material. A visible luminescence study indicated that the annealing process diminishes the presence of native defects that can act as bulk-like nonradiative centers that impact the UV luminescence.

An initial study of gallium oxide (Ga_2O_3) thin films was performed to determine the optical properties of this ultra-wide bandgap semiconductor. β-Ga_2O_3 thin films were grown via RF sputtering in two growth environments with different oxygen concentrations. Prior to characterization, a post growth annealing step was accomplished. An oxygen-rich growth environment resulted in highly defective films that resulted in broad, intense photoluminescent (PL) emissions accompanied by a weak deep ultraviolet peak. Adjustment to a lower oxygen content during growth resulted in higher quality films that display five resolved PL peaks in the UV range, including band edge emissions of ~ 4.85 eV that match the band edge values obtained via transmission spectroscopy. Additional peaks at ~ 3.14 eV and ~ 3.56 eV were attributed to donor-acceptor recombination and self-trapped hole

emissions, respectively. Designation of the self-trapped hole emissions at ~ 3.56 eV was verified by its absence in the PL spectra when sub-bandgap 3.8 eV excitation is used. Post-growth annealing in an oxygen environment instead of in air resulted in a blue shift of the PL spectra of ~ 120 meV and decreased the intensity of the ~3.56 eV STH related peak. These results indicate that the defect concentration in these films is highly sensitive to their oxygen content, which makes this material ideal for use in oxygen sensing devices.

Acknowledgements

I would like to thank Dr. Leah Bergman for providing me with the opportunity to participate in this research, and for her guidance and support throughout this endeavor. Additionally, I would like to thank her for humoring my frequently misplaced ideas, and for patiently giving me new insights into my research.

I am also grateful for the direction provided by the members of my committee, Dr. Ruprecht Machleidt, and Dr. M. Grant Norton. Their suggestions and recommendations were invaluable contributions to this research.

During the course of this research, Dr. Dinesh Thapa was a consistent source of knowledge and experience in the lab. Dinesh always provided valuable insight in a patient and thoughtful manner, no matter how frequent my interruptions for odd questions or proposals might be. For this, I am extremely grateful.

I would also like to thank Dr. Jesse Huso for encouraging me to return to college for this experience. I am also appreciative to him for his willingness to answer any of the many wild questions that happened to come up during my work.

I am thankful to Amrah Canul for his assistance during this research. Throughout my time here, Amrah consistently brought a fresh perspective to my work that made me think a bit more deeply and clearly about my research than I otherwise might have.

Special thanks also goes to KarlaRose Erhard-Hudson for all of her help over the past several years. In addition to my frequent interruptions, KarlaRose was always the person to go to when no one else could figure out how a process or procedure worked at the university.

Additionally, I would like to thank Brian Petty for his assistance and advice on equipment fabrication for the experiments in this research. Without Brian's expertise and rapid response to my requests, this research would not have been possible.

Finally, thank you to Dr. Thomas Williams of the Electron Microscopy Center for his assistance teaching and interpreting the microscopy related information obtained in this work. The information he provided was valuable to my research, and inspired me to learn much more about this field than I would have otherwise.

This research was supported by the U.S. Department of Energy, Office of Basic Energy Sciences, Division of Materials Science and Engineering under award DE-FG02-07ER46386.

I would like to dedicate this work to my wife Sue.

Thank you for all of your encouragement and support.

Table of Contents

List of Figures

List of Tables

Chapter 1: Wide Bandgap Semiconductors

1.1 Introduction

Materials that exhibit wide bandgap semiconducting behavior are highly sought after due to their potential to act as a high performance alternative to current semiconducting technologies, and for their unique characteristics that could lead to new technological capabilities.[1,2] These materials have applications in the construction of optoelectronic devices such as optical sensors and solid state lasers, with unique capabilities that are impractical with materials that are widely utilized today.[3-7] In order to fully realize the potential of these novel materials, a greater understanding of their natural properties, along with methods for improving their performance must be achieved. That is the focus of this work.

Materials that are classified as wide bandgap semiconductors typically have a bandgap in the range of 2.0 – 3.4 eV.[8] Zinc oxide is a material that was studied in this work that falls within this category. Gallium oxide is another semiconducting material that was studied in this work. It is commonly assigned to the ultra-wide bandgap class of semiconductors, whose bandgap energies exceed 3.4 eV.[9]

1.2 Zinc Oxide (ZnO)

ZnO is a wide bandgap semiconductor with a direct bandgap of ~ 3.3 eV, and a deep excitonic level of ~ 60 meV.[8] This makes ZnO a highly efficient emitter of UV radiation at room temperature. This material naturally occurs in the wurtzite structure, which is shown in Figure 1.1. ZnO is also environmentally friendly, inexpensive, easy to obtain, and can be synthesized using a number of methods to produce a variety of nanostructures and thin films. All of these traits have made ZnO an extremely popular wide bandgap semiconductor material study.[10-13]

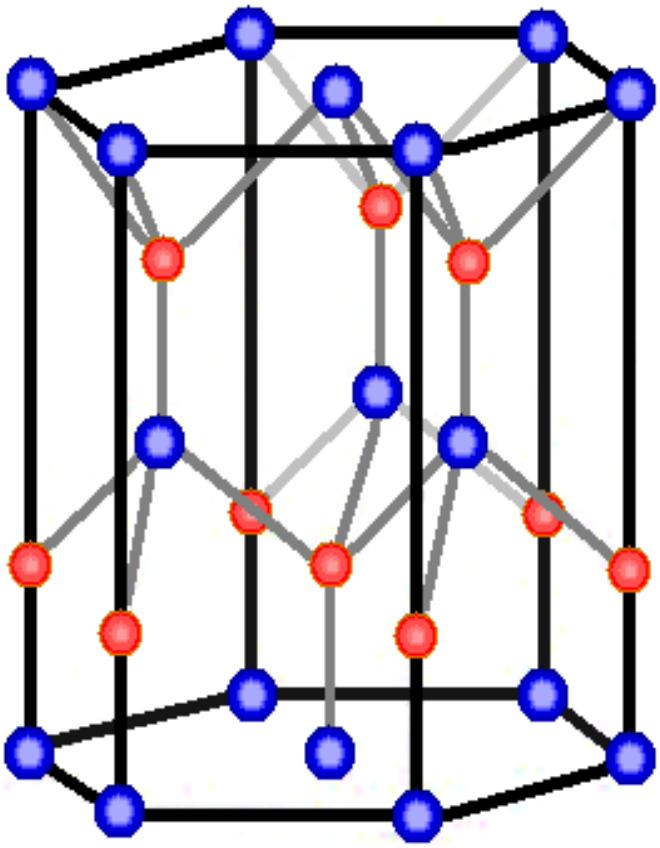

Figure 1.1 Wurtzite crystal structure of ZnO, with zinc atoms in blue, and oxygen atoms in red.[14]

1.3 Defect Limitations of ZnO Thin Films

One limitation of ZnO thin films that has been the subject of ongoing research is the presence of defects in ZnO that can diminish its luminescent properties. Nanocrystalline thin films possess a large surface to volume ratio. Large quantities of non-radiative centers, which diminish the luminescent intensity of the films, are the result of defects that reside on the granular film surfaces. ZnO film surfaces have a strong affinity to adsorb hydrogen and OH- groups from the environment. These adsorbates can act as traps to exited electrons and holes, resulting in a diminished band edge luminescence.[15] Additionally, native defects that reside in the volume of the sampled PL can also act as non-radiative centers, causing weak luminescence intensity.[10-12,16] A number of methods have been studied to remove or passivate these defects such as annealing and surface coating.

In studies related to the effects of surface coating, SiO_2 coating of ZnO nanowires has been found to increase the ultraviolet PL (UV-PL) due to the passivation of oxygen vacancies,[17] while the enhancement of the UV-PL in ZnO nanoparticles has been discussed in terms of the reduction of dangling bonds and O^{2-} ions due to SiO_2 capping.[18,19] Additionally, the weak UV-PL in ZnO quantum dots has been attributed to a $Zn(OH)_2$ shell covering the ZnO quantum dot.[20] If ZnO nanoparticles are capped by a polymer, a significant enhancement of UV-PL intensity has also been observed.[21]

A second approach to the enhancement of the UV-PL is annealing in controlled environments. Such treatments, if performed at an optimal temperature and in the proper environment, can suppress the effects of native defects and OH-groups, and improve the overall quality of the films.[8,10,11,15,20] Moreover, a detailed study of plasma cleaning of ZnO surfaces has demonstrated the importance of this treatment for the removal of hydrogen species.[24] In that study, the polarity of the ZnO surface was taken into account with regard to surface reconstruction after the cleaning.[22-24]

1.4 Gallium Oxide (Ga_2O_3)

Ga_2O_3 is a material that has generated a significant amount of recent research due to its potential for use in solar blind optical sensors and as a high-temperature gas sensor.[25,26,27] Ga_2O_3 occurs in a number of different crystal structures, but the most commonly studied is the β-phase, which is the most energetically stable phase.[27,28] A second, often studied variant of Ga_2O_3 is α-Ga_2O_3. α-Ga_2O_3, which exhibits the corundum crystal structure, and monoclinic β-Ga_2O_3, are shown in Figure 2.2, a) and b), respectively.[29] Theoretical studies of β-Ga_2O_3 have shown that this material has both a direct bandgap ($E_g = \sim 4.90 \pm 0.1$ eV), and an indirect bandgap ($E_g = \sim 4.85 \pm 0.1$ eV).[30] A literature review revealed that experimental verification of these values is sparse, so further experimental research is required to determine the nature of this material, which is a goal of the research performed in this study.

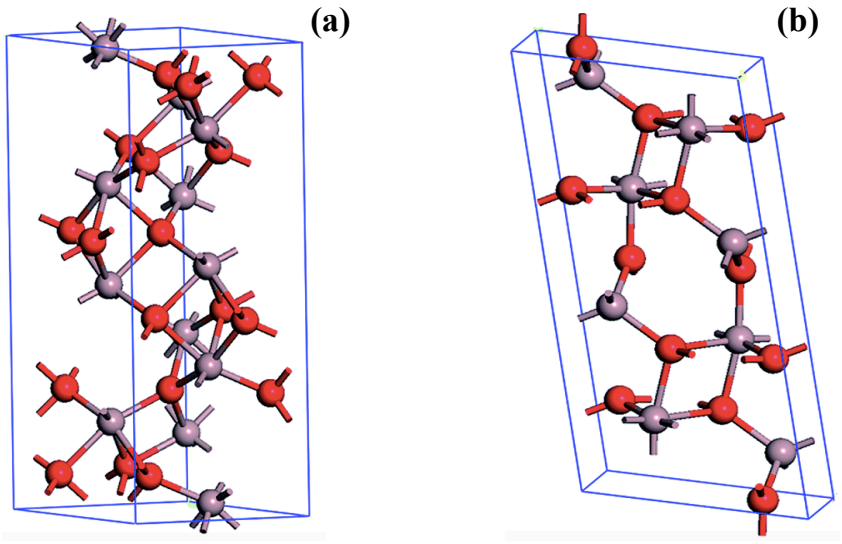

Figure 1.2 Crystal structure of (a) corundum α-Ga_2O_3, and (b) monoclinic β-Ga_2O_3, with oxygen atoms in red, and gallium atoms in gray. Ga_2O_3 is known to grow in three other phases, however, α-Ga_2O_3 and β-Ga_2O_3 are the most common phases. β-Ga_2O_3 is the most thermodynamically stable phase, and is the phase studied in this research.[29]

1.5 Self-Trapped Holes (STH) in Ga_2O_3

β-Ga_2O also has a high propensity to form self-trapped holes when electrons are excited from the valence band, causing most electron-hole recombination events to occur at a much lower energy level than a valence-to-conduction band transition would otherwise produce. STH occur due to deformation of the crystal lattice caused by an induced electric field that naturally occurs when holes are created in this material. It is more energetically favorable for holes to become self-trapped, than for the holes to remain in the valence band, leading to electron-hole recombination that produces a sub-bandgap emission.[31] The intrinsic STH property of Ga_2O_3 competes with the deep-UV light emissions (~ 5 eV), making this material most useful in UV technologies that require efficient emissions of ~ 3.5 eV .

1.6 References

1. X. Du, Z. Mei, Z. Liu, Y. Guo, T. Zhang, Y. Hou, Z. Zhang, Q. Xue, and A.Y. Kuznetsov, Adv. Mater. **21**, 4625 (2009).

2. G. Chen, F. Abou-Galala, Z. Xu, and B.M. Sadler, Opt. Express **16**, 15059 (2008).

3. N.J. Dayan, S.R. Sainkar, R.N. Karekar, and R.C. Aiyer, Thin Solid Films **325**, 254 (1998).

4. B.B. Rao, Mater. Chem. Phys. **64**, 62 (2000).

5. D.C. Reynolds, D.C. Look, and B. Jogai, Solid State Commun. **99**, 873 (1996).

6. Z.K. Tang, G.K.L. Wong, P. Yu, M. Kawasaki, A. Ohtomo, H. Koinuma, and Y. Segawa, Appl. Phys. Lett. **72**, 3270 (1998).

7. X.Y. Liu, C.X. Shan, H. Zhu, B.H. Li, M.M. Jiang, S.F. Yu, and D.Z. Shen, Sci. Rep. **5**, 13641 (2015).

8. D. Thapa, J. Huso, J.L. Morrison, C.D. Corolewski, M.D. McCluskey, and L. Bergman, Opt. Mater. **58**, 382 (2016).

9. J.Y. Tsao, S. Chowdhury, M.A. Hollis, D. Jena, N.M. Johnson, K.A. Jones, R.J. Kaplar, S. Rajan, C.G. Van de Walle, E. Bellotti, C.L. Chua, R. Collazo, M.E. Coltrin, J.A. Cooper, K.R. Evans, S. Graham, T.A. Grotjohn, E.R. Heller, M. Higashiwaki, M.S. Islam, P.W. Juodawlkis, M.A. Khan, A.D. Koehler, J.H. Leach, U.K. Mishra, R.J. Nemanich, R.C.N. Pilawa-Podgurski, J.B. Shealy, Z. Sitar, M.J. Tadjer, A.F. Witulski, M. Wraback, and J.A. Simmons, Adv. Electron. Mater. **4**, 1600501 (2018).

10. V.V. Khomyak, M.M. Slyotov, I.I. Shtepliuk, G.V. Lashkarev, O.M. Slyotov, P.D. Marianchuk, and V.V. Kosolovsky, J. Phys. Chem. Solids **74**, 291 (2013).

11. A. Singh, D. Kumar, P.K. Khanna, and M. Kumar, Mater. Lett. **183**, 365 (2016).

12. C.I.L. Sombrio, P.L. Franzen, R. dos Reis, H.I. Boudinov, and D.L. Baptista, Mater. Lett. **134**, 126 (2014).

13. L. Guo, S. Yang, C. Yang, P. Yu, J. Wang, W. Ge, and G.K.L. Wong, Appl. Phys. Lett. **76**, 2901 (2000).

14. J.L. Morrison, Luminescent MgZnO Nanoalloys, Master's Thesis, University of Idaho, 2006.

15. H. Idriss and M.A. Barteau, J. Phys. Chem. **96**, 3382 (1992).

16. L. Lin, J. Liu, J. Lv, S. Shen, X. Wu, D. Wu, Y. Qu, W. Zheng, and F. Lai, J. Alloys Compd. **695**, 1523 (2017).

17. C.I.L. Sombrio, P.L. Franzen, R. dos Reis, H.I. Boudinov, and D.L. Baptista, Mater. Lett. **134**, 126 (2014).

18. K.S. Babu, A.R. Reddy, and K.V. Reddy, Mater. Res. Bull. **49**, 537 (2014).

19. Z. Fu, B. Yang, L. Li, W. Dong, C. Jia, and W. Wu, J. Phys. Condens. Matter **15**, 2867 (2003).

20. H. Zhou, H. Alves, D.M. Hofmann, W. Kriegseis, B.K. Meyer, G. Kaczmarczyk, and A. Hoffmann, Appl. Phys. Lett. **80**, 210 (2002).

21. L. Guo, S. Yang, C. Yang, P. Yu, J. Wang, W. Ge, and G.K.L. Wong, Appl. Phys. Lett. **76**, 2901 (2000).

22. Y. Dong, Z.-Q. Fang, D.C. Look, D.R. Doutt, G. Cantwell, J. Zhang, J.J. Song, and L.J. Brillson, J. Appl. Phys. **108**, 103718 (2010).

23. F. Ostendorf, S. Torbrügge, and M. Reichling, Phys. Rev. B **77**, 41405 (2008).

24. B. Meyer, Phys. Rev. B **69**, 45416 (2004).

25. B.R. Tak, V. Gupta, A.K. Kapoor, Y.-H. Chu, and R. Singh, ACS Appl. Electron. Mater. **1**, 2463 (2019).

26. S. Li, S. Jiao, D. Wang, S. Gao, and J. Wang, Journal of Alloys and Compounds **753**, 186 (2018).
27. R. Jangir, S. Porwal, P. Tiwari, P. Mondal, S.K. Rai, T. Ganguli, S.M. Oak, and S.K. Deb, Journal of Applied Physics **112**, 034307 (2012).
28. Y. Yao, S. Okur, L.A.M. Lyle, G.S. Tompa, T. Salagaj, N. Sbrockey, R.F. Davis, and L.M. Porter, Mater. Res. Lett. **6**, 268 (2018).
29. M-G. Ju, X. Wang, W. Z. Liang, Y. Zhao, and C.Li, J. Mater. Chem. A **2**, 16892-16897 (2014).
30. H. Peelaers, H. and C.G. Van de Walle, Phys. Status Solidi B **252**, 828-832 (2015).
31. J.B. Varley, A. Janotti, C. Franchini, and C.G. Van de Walle, *Phys. Rev. B* **85**, 081109 (2012).

Chapter 2: Thin Film Synthesis

2.1 Thin Film Growth and Treatment Methods

The thin film materials that were studied in this work were grown using the sputtering process. Annealing was performed as a post-growth treatment of the films. This chapter discusses the background of sputtering, and the film growth and treatment processes used in this study.

2.2 Sputtering

Sputter deposition is a process that is frequently utilized to produce a broad range of materials in research and industry. This process is favored in industry due to the wide variety of materials, including alloys, that can be deposited, the low vacuum conditions required for successful deposition, and the near stoichiometric deposits that can be obtained. Additionally, objects of all sizes can be sputter coated rapidly with high quality coatings. Sputtering is used in a variety of applications, including glass coatings for enhanced thermal performance, anti-reflective optics, and as in this study, for the production of semiconductor films.[1]

2.2.1 Overview of Sputtering

Thin film sputtering is, in its simplest form, the transfer of a desired material from a bulk-like target via a plasma, to a substrate where it grows in a thin film form. A depiction of the sputtering process is shown in Figure 2.1. A sputtering system consists of an anode and a cathode that are situated in opposing positions in a vacuum chamber. In a system utilizing a DC power source, the target material is placed on the negative cathode, while the substrates where the films are to be deposited are placed on the positive anode. The chamber is then placed under vacuum and a process gas, which is typically argon or another heavier noble gas, is introduced into the chamber. Once a desired pressure and gas flow rate are reached, power is applied to the cathode, resulting in a strong electric field between the target and the substrate. The process gas is then ionized and accelerated toward the target. Upon impact

with the target, material is ejected from the target by the ionized gas and propelled toward the substrates, where it is deposited. The continued bombardment of the target by the process gas and subsequent deposition leads to the formation of a thin film of the desired material on the substrate.[2]

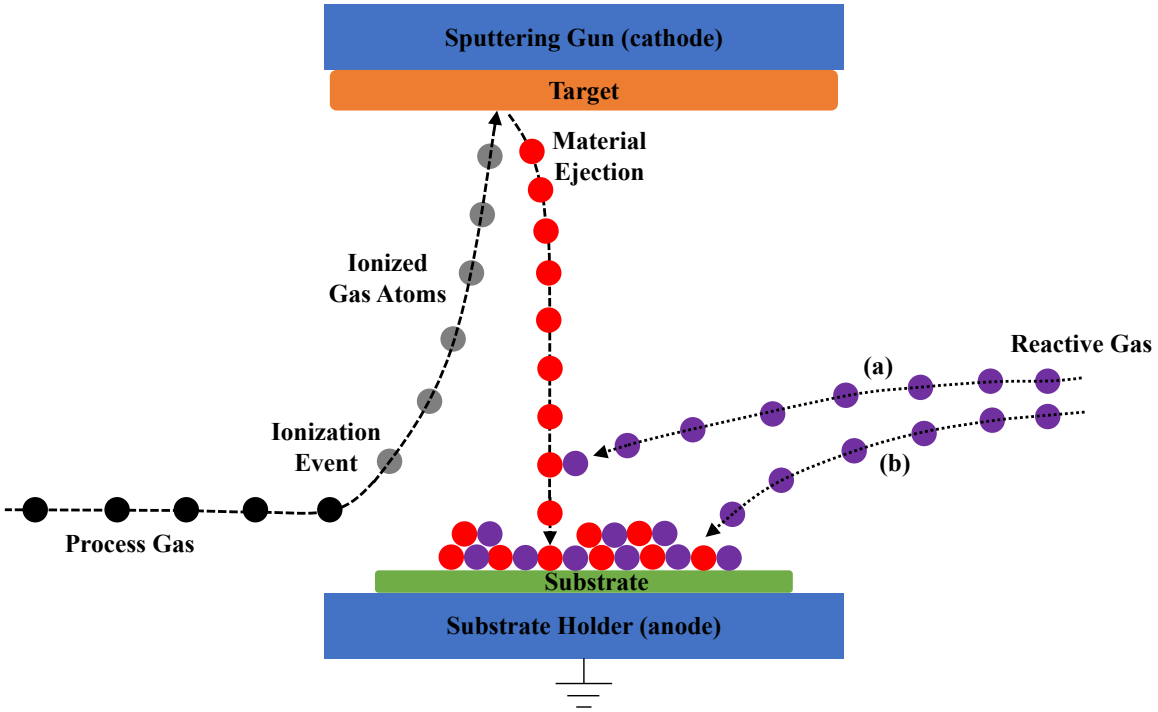

Figure 2.1 Schematic of the reactive sputtering process. The process gas enters the chamber and is ionized either from the electric field or from free electrons in the plasma. Following the ionization event, the ionized gas atoms are accelerated toward the target. The ionized gas atoms collide with the target, ejecting material from the target to be deposited onto the substrate. The reactive gas either, (a), bonds with the ejected material in the plasma column, or (b), bonds with the materials after deposition to form the desired compound. Standard, non-reactive sputtering follows the same process, but the reactive gas is not present. Some level of reactive gas was introduced into the growth environment for all of the materials in this research in order to maintain stoichiometric growth.

The custom sputtering system used for growth of the films in this work is shown in Figure 2.2. A more specific discussion of various techniques, components, and limitations of sputtering are in the following sections.

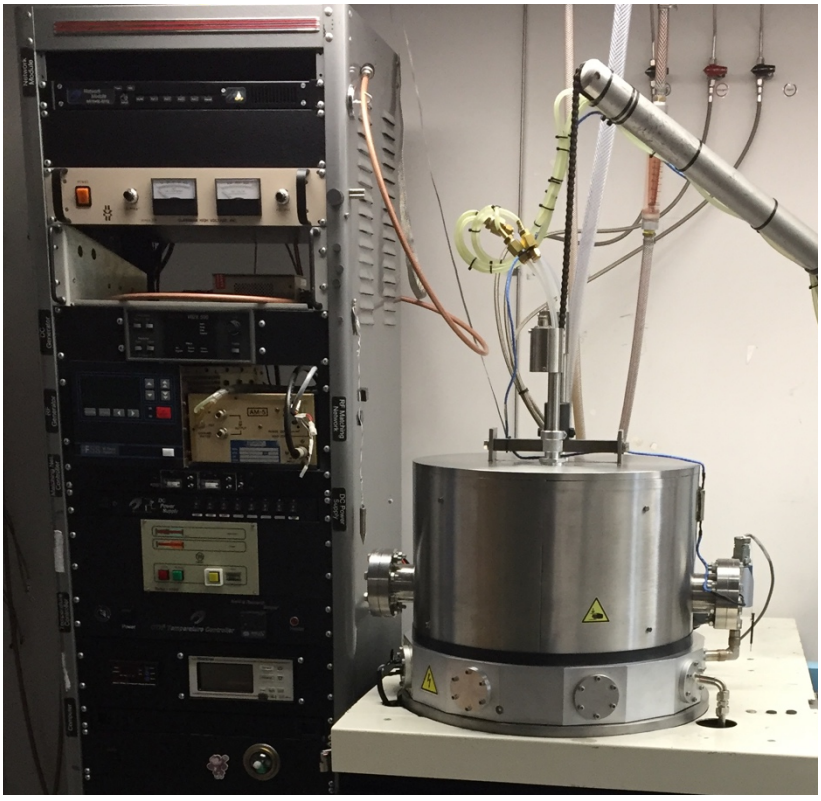

Figure 2.2 The sputtering system used for thin film growth in this research. The growth chamber is depicted on the right, and the associated system controls are located in the equipment rack in the left of the photo.

2.2.2 Substrate Selection and Heating

In most situations, and in all of the work for this study, substrates are required as a platform for growth of the film. Substrate materials are selected based on properties such as stability, resistance to heat, transparency in the desired range of the electromagnetic spectrum and crystal structure. In this work, sapphire, quartz and silicon substrates were chosen based on these properties and the past experience with these materials in the lab.

C-plane sapphire (Al_2O_3) substrates were used exclusively for work involving ZnO films. Previous work performed in the lab showed that the hexagonal crystal structure of these substrates is highly compatible with the ZnO films, and it was chosen for this reason. Due to the lack of previous work with Ga_2O_3 films, c-plane sapphire, z-cut quartz (SiO_2) and silicon (Si) (111) substrates were used to determine their performance.

A difficulty that is frequently encountered in film growth methods, including sputtering, is the disorder of the atoms, called adatoms, after deposition, which leads to poor

material performance. This disorder is caused by adatoms that once deposited, retain too little energy to arrange themselves in a more orderly fashion before subsequent adatoms are deposited, thus fixing them in an unfavorable position . Providing additional energy to the adatoms after they arrive at the substrate via heat is one method to partially overcome this problem.[3] In this work, the use of substrate heating for all materials was crucial to enhance the performance of the films.

In this research, the sapphire substrates used in the ZnO and coating research were heated to 250º C, unless otherwise noted. In the case of the Ga_2O_3 samples, substrates were heated to 400º C. In all instances, the chamber remained under high vacuum of ~$3*10^{-5}$ torr while the substrate temperature was greater than 100º C to prevent annealing effects from impacting the as-grown nature of the samples.

2.2.3 Reactive Sputtering

In standard sputtering, the target material is the same as the desired film material, but the target material is in a bulk form. In contrast, the deposited material is in a film form, and can possess very different properties. In many instances the desired material is either difficult or prohibitively expensive to obtain in a target form, or the material is too fragile in target form to be sputtered. One alternative for some materials is to perform deposition using reactive sputtering. In reactive sputtering, the target material is an elemental constituent of the desired film, such as Zn in our ZnO films. During deposition, along with the process gas to be ionized, a second reactive gas, in our case O_2, is introduced into the plasma to react with the target material. For example, the reaction shown in (1), leads to the deposition of the desired ZnO film.[1]

$$2\,Zn^{2+} + O_2 \longrightarrow 2\,ZnO \qquad (2.1)$$

2.2.4 DC vs RF Sputtering

At this point in the discussion of sputtering, the power supplied to the cathode has been assumed to be direct current, or DC. In this type of sputtering, the cathode is held at a constant fixed potential with respect to the anode. DC sputtering is useful for depositing materials such as metals that have a high electrical conductivity. It also requires less

equipment, and generally has a higher deposition rate than its RF counterpart. Films deposited via DC sputtering typically exhibit lower quality due to the higher deposition rate, which limits the ability of deposited adatoms to rearrange prior to subsequent deposition. The higher impact energies of the adatoms onto the sample surface during DC sputtering deposition can also result in lower film performance.[1] Additionally, the accumulation of positively charged ionized gas molecules on the target surface can shield newly ionized gas molecules from reaching the surface of the target, which reduces the deposition rate. This phenomenon is called target poisoning, and its effects vary based on the type of target material and become more pronounced over long deposition times.[1,4]

A method to overcome the limitations associated with DC sputtering, is to deposit material using a RF power source connected to the sputtering gun where the target is located. The RF source alternates the potential of the target with respect to the substrates at a frequency of 13.56 MHz. This alternates the direction of the electric field within the plasma at the same rate. The advantage of using RF sputtering is that target poisoning is eliminated due to the fluctuation of the electric field. Additionally, charged atoms in the plasma are subject to this alternating electric field as well, resulting in lower adatom impact energies at the substrates and slower deposition rates. These factors typically result in the deposition of higher quality films, although the deposition rate of most materials is approximately 50% of the DC rate for the same material deposited at the same power. RF sputtering also allows for deposition using both conductive and nonconductive targets, broadening the applicability of this deposition method.[2]

2.2.5 Magnetron Sputtering

The introduction of a magnetron into the sputtering system can dramatically improve the efficiency of the sputtering process. A magnetron sputtering gun consists of a standard sputtering gun with magnets arranged in a circular pattern on the mounting surface of the gun. When the target is placed on this surface and the plasma is initiated, free electrons from the ionization of the process gas are trapped near the outer surface of the target. This creates increases the negative charge near the target and creates a “screen” of electrons that the ionized process gas must pass through to reach the target surface. The trapped electrons collide with the process gas to cause a greater percentage of the gas to be ionized, resulting in

higher sputtering rates than a similarly configured non-magnetron system.[1] Magnetron sputtering can be used for conducting and non-conducting target materials, and was used exclusively in this research.

2.2.6 Sputtering Targets

The source of the material that is ultimately deposited on the substrate in a sputtering system is introduced to the system in the form of a sputtering target. Targets can be fabricated locally or purchased, depending on the requirements of the planned deposition. Metal targets are easily produced locally by pressing metal powder in a die into the form of a target. Metal targets, such as the Zn, Al, and Mg targets that were produced for this study, were formed from metal powder. In order to form the targets, the powder was placed in a 2" die, with a thickness of ~ 1/4", and placed in a shop press for ~ 24 hours at ~ 50 000 psi. Non-metallic targets, such as the Si, SiO_2, and Ga_2O_3 targets used in this research, are typically more fragile and difficult to produce, and were purchased from vendors that specialize in target fabrication.

2.2.7 Chamber Pressure and Process Gasses

As previously mentioned, in order to achieve a plasma strike and material deposition in a sputtering system, the sputtering system must be under vacuum and process gasses must be present to be ionized. Additionally, reactive gasses must be present for reactive sputtering or, in the case of some materials, to maintain a stoichiometric deposition composition. Prior to the introduction of process gasses and the start of deposition, the sputtering chamber is placed under high vacuum to ensure any residual contamination is removed from the chamber. At these low pressures, the lack of sufficient numbers of gas molecules requires the introduction of a process gas. In order to achieve an optimal sputtering rate, the pressure must be high enough for sufficient numbers of gas molecules to be ionized in order to maintain the plasma. However, if the pressure is too high, ionized gas molecules will be prevented from impacting the target due to collisions with the excess non-ionized gas molecules present in the chamber. This optimum point varies slightly based on the target material and the gasses present in the chamber.[1,2] Variations from this optimum point slow the deposition rate and can require the sputtering power to be increased, resulting in greater

risks for target and equipment damage. Once the optimum pressure and gas composition is reached, power can be applied to the sputtering gun, and deposition can commence.

In this research, the primary process gas used for ionization was Ultra High Purity (UHP) argon gas. Argon(Ar) was selected since it is a relatively heavy noble gas, making it easy to ionize with enough mass to provide reliable material ejection from the target upon impact. Additionally, Ar is readily available and inexpensive when compared to other gasses with similar properties. The other process gas used in this research was UHP oxygen (O_2). This gas was used for reactive sputtering of ZnO, MgO, Al_2O_3, and SiO_2 films in a Ar:O_2 environment of 3:1. UHP O_2 was also used for Ga_2O_3 deposition in an Ar:O_2 ratio of 70:1 due to the propensity of Ga_2O_3 to lose oxygen during growth.[5] For the system and all of the materials used for this research, initial pre-deposition pressure was less than $8*10^{-5}$ torr, and the working pressure was set to ~ $1.2*10^{-2}$ torr.

2.3 Annealing

Annealing is a post-growth process that involves heating a material to a high temperature in a specific environment to improve the arrangement of the atoms into a more crystalline from than can be achieved through the growth process alone. Annealing typically improves the performance of the materials by removing defects such as vacancies and interstitials, while increasing the size of the crystals, or grains, in the films.

2.3.1 Annealing Temperatures and Times

Heat is used as an effective means to rearrange atoms into a more organized crystal structure that produces a better performing material. The temperature at which annealing is conducted, and its duration, can significantly affect the properties of the material. If the temperature is too low, the energy imparted to the atoms is insufficient to promote proper reordering of the atoms into an ideal crystal structure. Similarly, if the duration of annealing is too short, the atoms are unable to rearrange completely before the energy drops and the atoms are locked into an imperfect structure. Conversely, adding too much energy through too high of an annealing temperature can cause the atoms to rearrange into an entirely new, undesired structure, or even cause an excessive loss of material. The primary drawback of extremely long annealing times is the waste of resources.[2] In this work, ZnO films were

annealed at 900º C for 60 minutes unless otherwise specified. This temperature and time was selected based on previous experience in the lab. Ga_2O_3 samples were annealed at 1100º C for 180 minutes based on information from literature and preliminary trials conducted in the lab.[6]

2.3.2 Annealing Environments

The environment that a film is annealed in provides a source for the addition or removal of material from the sample. Annealing in an inert environment such as Ar can allow the film to rearrange to a more orderly structure without the introduction of additional chemical species that could interfere with the performance of the material. However, if a film has an excess of vacancies, the inert gas in the environment is unable to effectively fill the vacancies, and does not improve the characteristics associated with these defects. In more reactive environments such as air or O_2 the chemical species in the environment will more readily become part of the sample, which provides a mechanism for filling vacancy defects. The higher reactivity of these environments can also help to remove contaminants due to their ability to bind readily with the contaminants during annealing. A drawback to these highly reactive environments is that they are more prone to adding undesirable chemical constituents to the films such as excess oxygen, nitrogen, or carbon.[7] The ideal environment for each material is selected based on its traits and the desired characteristics of the material post-processing. In this work, annealing of the ZnO samples was performed in an Ar environment. This decision was based on previous work in the lab that showed an Ar environment was preferred for optimal photoluminescent intensity in ZnO films. The Ga_2O_3 films were annealed in air and O_2 environments based on information in literature and initial lab trials.[6]

2.4 References

1. M. Ohring, *Materials Science of Thin Films: Deposition and Structure*, 2nd Ed. (Academic Press, San Diego, 2002) pp 204 – 217.
2. D.L. Smith, *Thin-Film Deposition: Principles and Practice*, 2nd ed. (McGraw-Hill, New York, 1995) pp 119, 431-434.
3. C. Koerner, C. Elschner, N.C. Miller, R. Fitzner, F. Selzer, E. Reinold, P. Bäuerle, M.F. Toney, M.D. McGhee, K. Leo, and M. Riede, Org. Electron. **4**, 623 (2012).
4. D. Depla and R. De Gryse, Surf. Coat. Technol. **2-3**, 184 (2004).
5. L. Dong, R. Jia, B. Xin, B. Peng, and Y. Zhang, Sci. Rep. **7**, 40160 (2017).
6. A.K. Saikumar, S.D. Nehate, and K.B. Sundaram, ECS J. Solid State Sci Technol. **8**, Q3064 (2019).
7. G. Fu, A. Polity, N. Volbers, B.K. Meyer, Thin Solid Films **4**, 2519 (2016).

Chapter 3: Thin Film Characterization

3.1 Thin Film Characterization Methods

The films produced for this research were characterized using photoluminescence (PL) , Raman, and transmission spectroscopy. Additionally, scanning electron microscopy (SEM) was used to image the films. This chapter provides background information about each of these techniques, and the general parameters used for each technique in this research.

3.2 Photoluminescence

When an electron in a material is excited via an incident light source with sufficient energy to reach a higher energy level, the electron will attempt to return to a more favorable energy state. This is often referred to as electron-hole recombination. Electron-hole recombination results in the emission of a photon with a specific energy that is indicative of a specific property of that material. The entire process of electron excitation via a light source, followed by the subsequent recombination and light emission is called photoluminescence (PL), and it is a non-destructive method of studying a variety of properties of luminescent materials. Photoluminescence can provide information about the material such as the bandgap emission energy or various other recombination processes. In many instances additional emissions related to the presence of impurities or defects are observed.[1]

Ideally, when a material is subjected to an excitation energy greater than the bandgap of the material, photoluminescence will result in the observation of a single narrow energy range, intense emission indicative of a conduction-to-valence band electron-hole recombination event. In the experimental, non-ideal case, emissions are over a broader energy range, less intense and vary in energy from the ideal case. This is due to the presence of defects, impurities, and coulombic interactions between the electron hole pair after excitation. Greater concentrations of defects and impurities in the material will result in greater deviation from the ideal case, making the material a less efficient emitter.[1] This is important for applications such as LEDs and lasers, where high efficiency emission is required for a material to be useful. Figure 3.1 depicts various possible recombination scenarios for a typical semiconducting material.

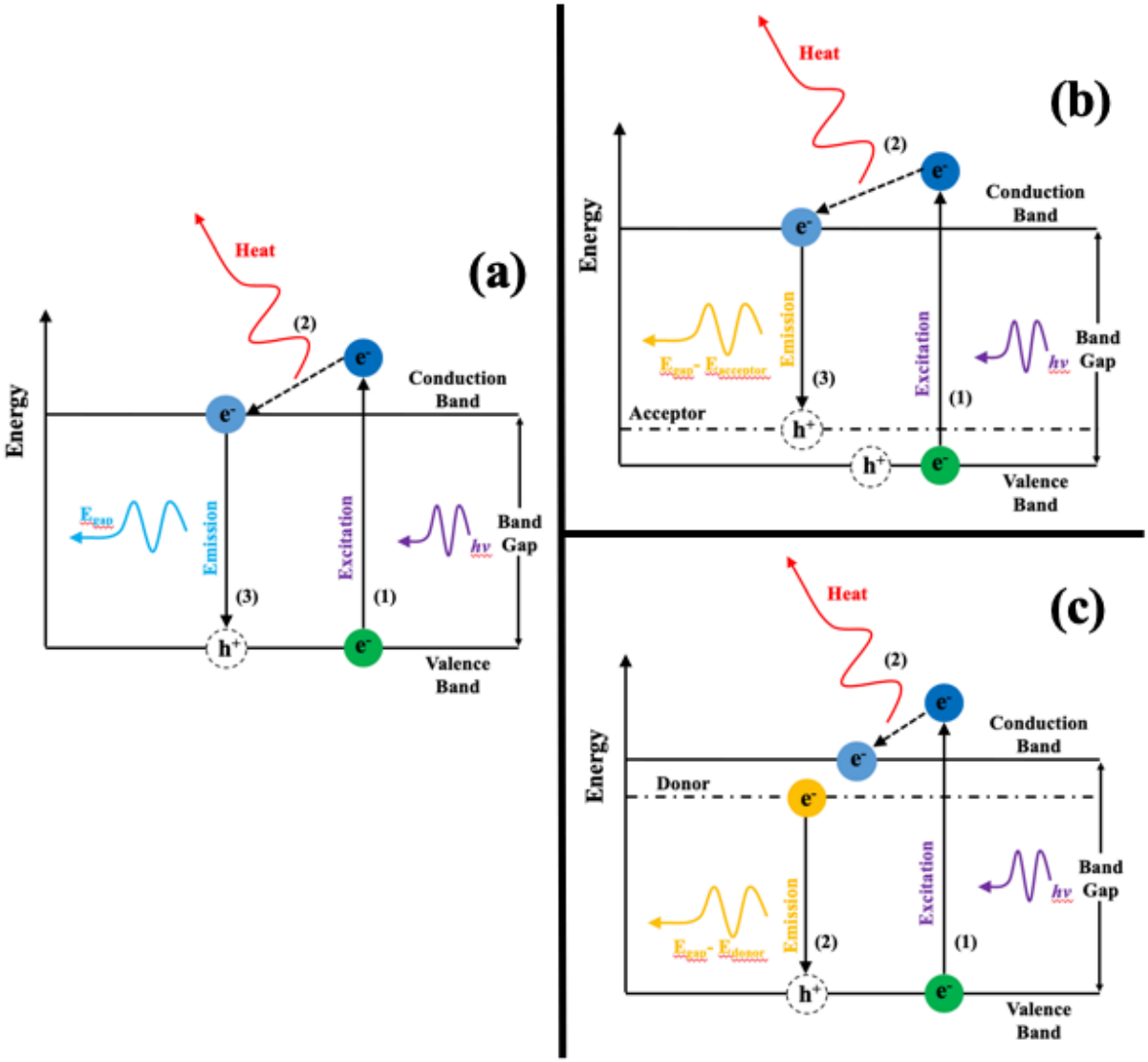

Figure 3.1 Common electron-hole recombination scenarios that result in PL emissions. (a) Band edge emission occurs when the incident excitation energy excites an electron above the bandgap (1). As the electron relaxes to the conduction band, heat is radiated (2). The electron in the conduction band then recombines with a hole in the valence band, resulting in the emission of light with the same energy as the bandgap (3). (b) The presence of impurities, crystal defects, or other material properties can result in an alternative recombination path, where available holes exist at energies higher than the valence band energy. This results in a lower efficiency optical material due to the sub-bandgap emissions that occur. (c) Impurities and defects can also cause a donor level, where electrons residing at an energy level lower than the conduction band also cause sub-bandgap emissions.

In this research, photoluminescence measurements were performed to achieve two primary goals. In the case of the ZnO films, the development of a process to improve the intensity of the luminescent emissions near 3.3 eV was the goal of the research. PL measurements were performed to quantify the results of this work. In the case of the Ga_2O_3 research, PL was used to determine if deep UV band edge emission could be observed. It was also used to determine if sub-bandgap emissions occur in this material and the mechanisms that are responsible for these emissions.

The PL measurements for this work were performed using two different methods, based on the emission energy of the material and the goal of the experiment. Micro UV-PL spectra were obtained with a Jobin-Yvon T64000 system, depicted in Figure 3.2, using 5.1 eV (244 nm) or 3.8 eV (325 nm) laser excitation. Visible PL measurements on the ZnO were performed using a JY-Horiba Fluorolog-3 spectrophotometer with Xe lamp excitation.

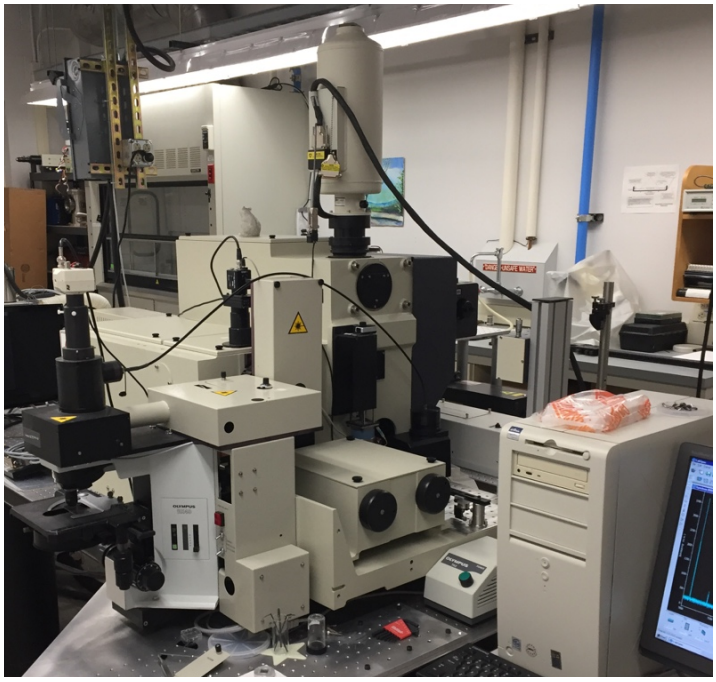

Figure 3.2 Jobin-Yvon T64000 micro-Raman/PL system used to obtain Raman and PL spectra in this research. The system is equipped multiple laser excitation sources in the UV range of the electromagnetic spectrum. In this research, the ZnO coated films were excited using a 3.8 eV (325 nm) laser, and excitation of the Ga_2O_3 films was performed with a 5.1 eV (244 nm) laser in most instances. The excitation laser power in most of the experiments was ~ 32.5 mW.

3.3 Raman Spectroscopy

Raman spectroscopy is a highly sensitive characterization technique used in conjunction with PL that measures the vibrations induced by an incident light source into the crystal structure of the material. Properties such as the structure of the crystal and the bond energies of the material under test can be determined via Raman spectroscopy. Raman scattering occurs when an incident photon inelastically scatters off of an atom in the crystal, a portion of the energy from the collision is converted into vibrations in the crystal lattice, called phonons. Figure 3.3 depicts the Raman scattering of an incident photon and the creation of a phonon in the crystal lattice. The energy of the phonons can be approximated as a harmonic oscillator that follows the relation[2]:

$$v = \frac{1}{2\pi c}\sqrt{\frac{k}{\mu}} \tag{3.1}$$

where v is the energy of the phonon, k is the "spring constant" of the bond, and μ is the reduced mass of the atoms associated with the vibration.

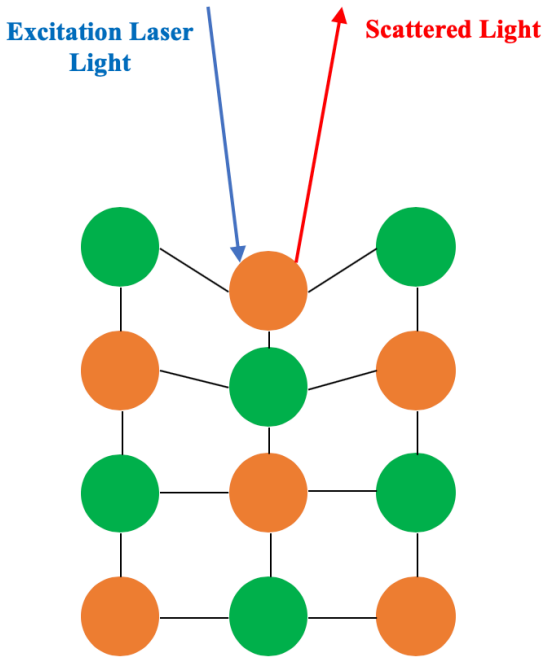

Figure 3.3 Incident laser light strikes the crystal lattice and is scattered back to the photodetector. The inelastic scattering event is called Raman scattering, and it imparts a small amount of energy into the crystal lattice in the form of vibrations called phonons. Phonon energy can be measured using conservation of energy by calculating the difference between the incident and scattered photon energy.

Alternatively, the phonon energy can be determined by measuring the energy of the incident photon before and after the scattering event. The difference in energy between the incident and the scattered photon is the energy of the phonon, *v*. This is the method used to measure phonon energy experimentally.

Due to the nature of the Raman scattering process, Raman spectroscopy is highly sensitive to differences in crystal structure and stress/strain in a crystal. In this work Raman spectroscopy was used to determine the stress/strain relationships between the ZnO films and coatings. It was also used to identify the material and crystal structure present in Ga_2O_3 films when x-ray diffraction signals could not be obtained. Micro-Raman spectra were obtained with the same Jobin-Yvon T64000 system, depicted in Figure 3.2, that was used for the PL spectra with 5.1eV (244 nm) or 3.8 eV (325 nm) laser excitation.

3.4 Transmission Spectroscopy

Transmission spectroscopy is a commonly used technique that tests the ability of a material to allow light to pass through it over a broad range of wavelengths. This characterization method relies on the fact that a material allows light with energy lower than its bandgap to pass through, while light with energies greater than the bandgap are blocked. Due to this property of materials, transmission spectroscopy can be used to observe the bandgap of a material that would otherwise be unobservable using PL, since some materials do not produce bandgap emissions. However, this method of testing does not provide information about sub-bandgap material emissions as in PL, since this technique simply measures the amount of light that passes through a sample. Another limitation of this technique, when applied to thin film material testing, is that the bandgap of the substrate must be higher than the highest light energy in the testing range. Failure to take this limitation into account will cause extraneous information about the substrate to interfere with data about the material due to the opacity of the substrate at energies above its bandgap.

In this work, transmission testing was performed using the Agilent Cary 300 UV-Vis spectrophotometer shown in Figure 3.4. This testing was conducted for two purposes. The first was to determine the bandgap of the Ga_2O_3 thin films. Once the transmission spectrum was collected, further analysis was conducted to find the derivative of the spectrum. By analyzing the derivative, the bandgap could be determined, since the energy where the

derivative is a minimum corresponds to the bandgap of the material. Additionally, transmission spectra were used to verify that the coatings applied to the ZnO films were non-reflective since Al and Mg were reactively sputtered onto the ZnO surface. The substrates used for transmission measurements were Al_2O_3 and SiO_2, whose bandgaps are ~ 8.8 eV and ~ 9.0 eV, respectively.[3,4] This is well above the maximum 6.5 eV energy of the light used in the transmission scans.

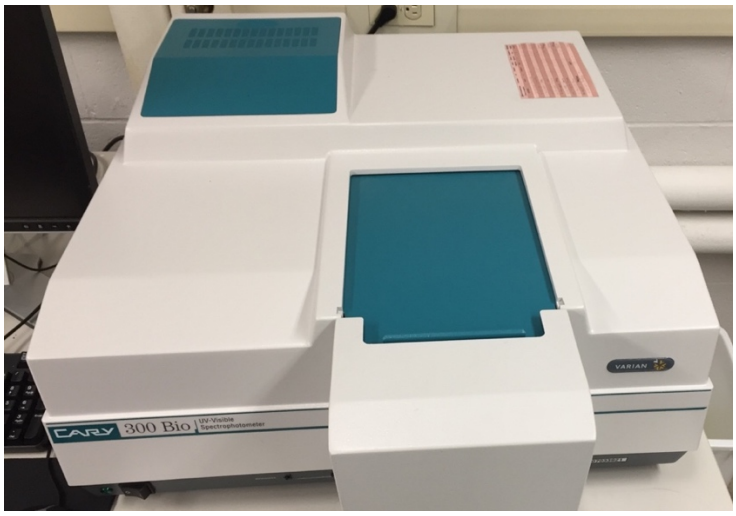

Figure 3.4 Agilent Cary 300 UV-Vis spectrophotometer used for transmission spectra collected in this research. Spectra of the coated ZnO films were primarily used to detect transparency changes after coating deposition. Ga_2O_3 spectra were analyzed to determine the bandgap of the deposited films.

3.5 Scanning Electron Microscopy (SEM)

Scanning electron microscopy, or SEM, is a technique that uses a focused electron beam to provide an image of a material in much greater resolution than would be possible with standard optical microscopy due to the short wavelengths of the electrons. In a SEM, electrons emitted from an electron gun are directed at the material under test in a raster, or scanning, pattern. The electrons are directed to the surface of the material in an electric field with potentials that generally range from 5 kV to 50kV. Upon striking the surface, the electrons encounter both inelastic and elastic scattering, both ejected to the detectors, with each type providing different images of the material and requiring different detector configurations. Additionally, x-rays from electron relaxation events are emitted from the sample with energies that are unique to specific elements. Measurement of the energy of the

x-rays can be used to produce a compositional map of the sample.[5] A diagram of the typical SEM configuration and the associated detectors discussed below is shown in Figure 3.5.

Inelastic scattering events occur with enough energy to either eject an electron from the material, or cause a cascading electron excitation chain until an electron is ejected from the material. These low energy secondary electron scattering events are commonly referred to as SE events, and are followed by the number of scattering events before an electron is emitted from the surface. For example, when an electron strikes the sample, exciting an electron, which is then emitted from the material, the event is called an SE1 event, when two scattering events occur, the event is called an SE2 event.[5]

Since SE1 events only allow for a single scattering event before ejecting a material from the surface, SE1 events are primarily confined to the surface of the material. Additionally, the electrons in an SE1 event are emitted at an angle close to normal with the surface of the sample. In order to detect electrons emitted in SE1 scattering events a detector is placed in line with the electron gun. This detector, called an in-lens detector, is typically placed at a small working distance from the sample and the electron gun is operated at powers less than 5kV. The in-lens detector provides a highly magnified two-dimensional image of the surface of the sample.

Secondary scattering events denoted SE2 and above occur most frequently at, or slightly below the surface (less than 1 nm) of the sample and the electrons are emitted from the material at angles well away from normal to the sample surface. Due to the angle of electron emission in this type of event a detector, called an SE2 detector, is placed as shown in Figure 3.5. When compared to in-lens imaging, SE2 imaging is typically performed at longer working distances of 3 mm to 10 mm, and higher powers of 10kV to 30kV. Due to the offset angle and the type of emissions detected, the SE2 detector is capable of producing high resolution surface images of the sample that include depth-related information.[5,6]

Elastic scattering, or backscattering, events are high energy scattering events where the incident electrons interact with the nucleus of the atoms in the sample and are scattered directly out of the sample. The probability of the occurrence of these events increases as the atomic number of the scattering atom increases, so compositional differences in different regions of a sample can be detected by observing these events. The variation between elements is given as[5]:

$$P \propto 0.05Z^{\frac{1}{2}} \tag{3.2}$$

where P is the probability of scattering and Z is the atomic number of the element. Domains with lighter colors indicate the presence of elements with a higher average atomic number, while darker domains contain elements with lower average atomic numbers.

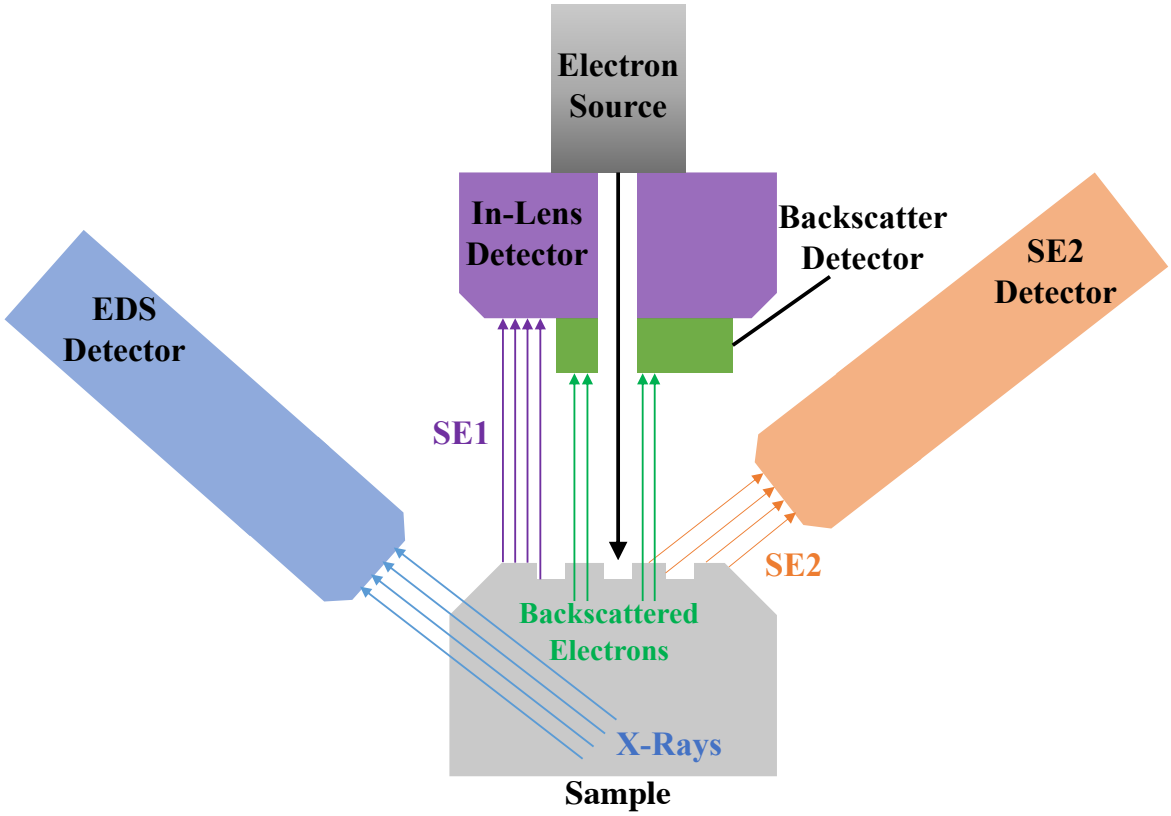

Figure 3.5 A typical SEM configuration, with the electron source and the various detectors utilized in this research. The excitation electrons are emitted from the electron gun, as represented by the black arrow. Various emissions are emitted from a tear-drop shaped volume of the sample. The in-lens detector produces a 2-D surface image from singly scattered electrons (SE1), shown in purple. The SE2 detector collects multiply scattered electrons, shown in orange, that produce an image that include depth related features from the sample surface. Backscattered electrons, shown in green, are collected by the backscatter detector and originate from deeper within the sample. These electrons vary in energy based on the atomic number (Z) of the atom involved in the elastic scattering event. The EDS detector collects x-rays, shown in blue, that originate from the deepest region of the excitation volume, and provide the elemental composition of the sample based on the emitted wavelength.

Unfortunately, this variation is not significant enough to perform elemental identification from backscattering events. Due to their high energy, backscattering events can occur much deeper (up to ~ 500 nm) within the sample than SE events, so information about compositional differences through a large cross section of the sample can be observed. In order to observe backscatter events with an SEM, a backscatter detector is inserted into the SEM at an angle near normal to the sample surface. A depiction of the inelastic, elastic, and backscatter events is shown in Figure 3.6.[5]

A final type of detector, often used in conjunction with an SEM, is called an x-ray energy dispersive detector (EDS). Excitations of electrons from the incoming electron beam and subsequent inelastic scattering events produce x-rays due to electrons relaxing back to their original energy states. The x-rays detected from these events can originate up to 1 μm below the sample surface, so for the films in this study, the entire cross section of the film is sampled. These x-rays are characteristic of the atom type and can be used to determine the types of atoms present in the sample and the concentrations of these atoms in the sample. Additionally, through the use of a technique called EDS mapping, a map of the concentrations of the constituent atoms throughout a region of the sample can be produced. The EDS detector is typically placed at an angle to the sample, similar to the SE2 detector, and used at moderate powers of ~10 kV with long working distances of ~10 mm.[5]

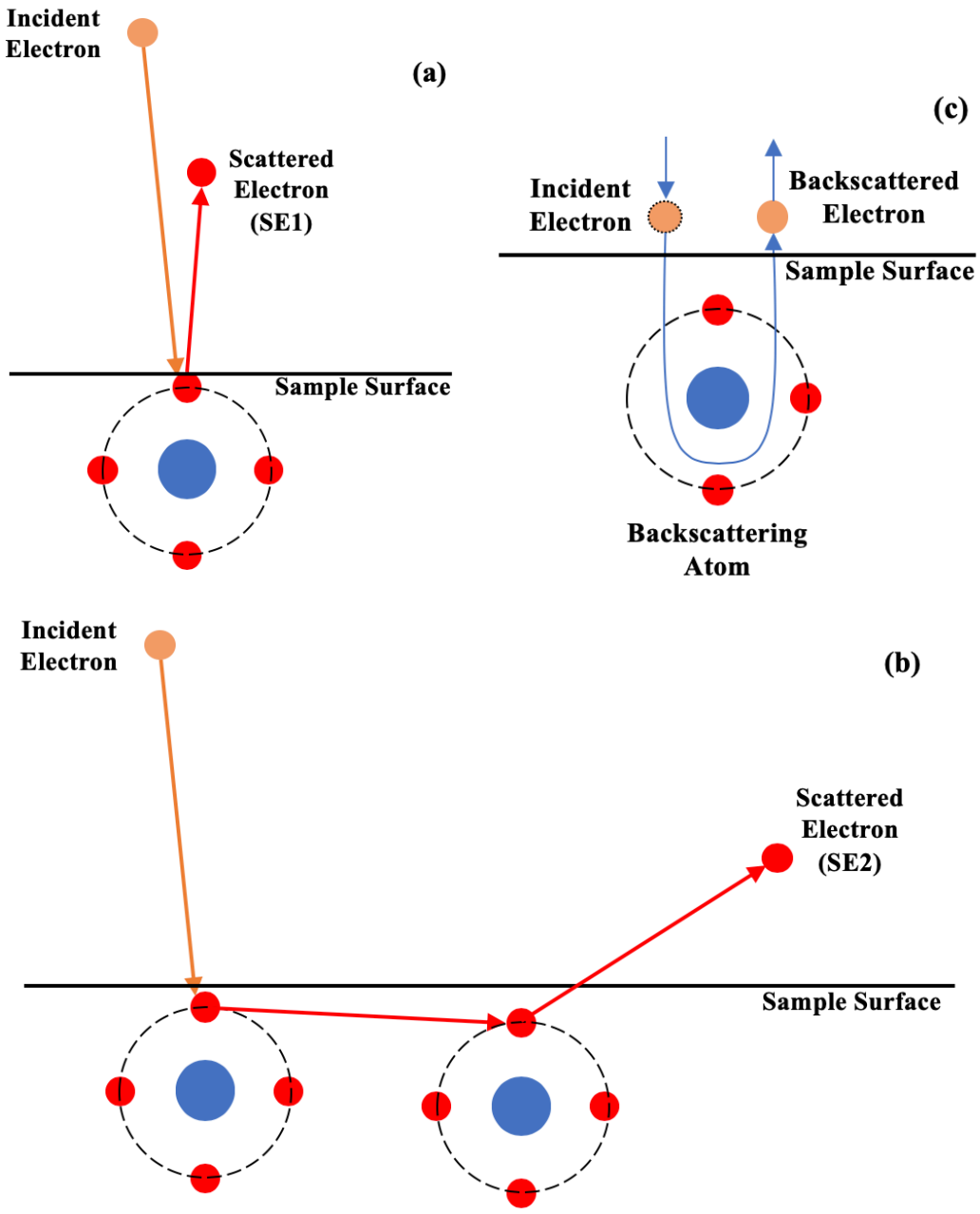

Figure 3.6 Electron emission mechanisms in a SEM. (a) depicts an SE1 event that emits an electron at a high incident angle. This type of emission consists of a single scattering event, and is detected by the in-lens detector. The process in (b) is an SE2 event where the incident electron inelastically collides with an electron in the sample and creates a scattering event. The scattered electron then undergoes a secondary inelastic event, which scatters another electron out of the sample. SE2 and higher order scattered electrons are ejected from the sample at lower angles than SE1 events, and are detected by the SE2 detector. Finally, the backscattering event depicted in (c) shows the incident electron being elastically scattered back out of the sample. The energy of the scattered electrons in these events are sensitive to differences in the atomic number (Z) of the backscattered atom, and can provide information about compositional differences in a sample.

3.6 References

1. D.L. Smith, *Thin-Film Deposition: Principles and Practice*, 2nd ed. (McGraw-Hill, New York, 1995) pp 568.
2. E. Smith and G. Dent, *Modern Raman Spectroscopy: a Practical Approach*, (J. Wiley, Hoboken, NJ, 2005) pp 79-82.
3. R.H. French, R.L. Coble, R.V. Kasowski, and F.S. Ohuchi, Physica B+C **1-2**, 47 (1988).
4. T.H. DiStefano and D.E. Eastman, Solid State Comm. **9**, 2259 (1971).
5. M. Ohring, *Materials Science of Thin Films: Deposition and Structure*, 2nd Ed. (Academic Press, San Diego, 2002) pp 583 - 589.
6. B.F. Griffin, Scanning **33**, 162 (2011).

Chapter 4: Optical Coatings for ZnO Thin Films

4.1 Coating Materials

In this research ZnO luminescent thin films were coated with various materials to address surface defects, and study their impact on the UV-PL intensity of the ZnO. A description of the selection criteria and properties of these materials follows in this chapter.

4.2 Material Selection Criteria

An ideal material for an optical coating that can enhance the UV-PL of ZnO should have the following properties:

- The bandgap of the material must be sufficiently higher than the energy of the light source used for excitation. If this is not the case, the coating will absorb the incident light, electrons in the underlying ZnO will not be excited, and photoluminescence will not occur.
- The interface between the coating and the ZnO should form a type 1 junction for optimal efficiency. The formation of a type 1 junction confines the excited electrons and holes to the ZnO material, leading to more efficient electron-hole recombination. A depiction of a type 1 junction is shown in Figure 4.1, and the band alignments of the materials selected is shown in Figure 4.2.[1,2]
- The coating material should be readily available, inexpensive and environmentally friendly. These material properties will make it more likely to be used for future applications in opto-electronic devices. Additionally, since the materials are to be deposited via sputtering, a method for sputtering the material must be available.
- The variation in average bond energy should be large enough that if a relation between the average bond energy of the coating material and the UV-PL intensity enhancement observed exists, it can be observed.

Based on these criteria, the materials used as coatings in this research were aluminum oxide (Al_2O_3), silicon dioxide (SiO_2), and magnesium oxide (MgO).

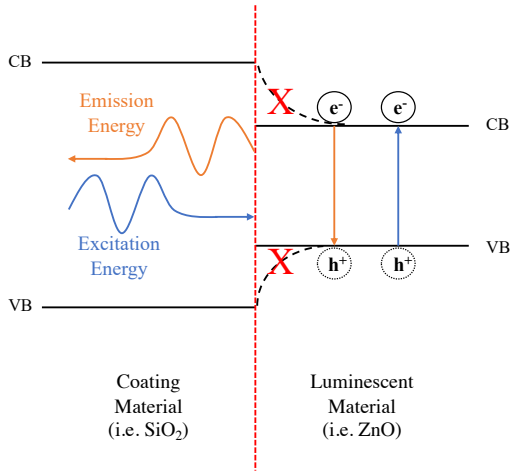

Figure 4.1 Diagram of a type 1 semiconductor junction. As incident light strikes the luminescent material, negatively charged electrons are excited to the conduction band (CB), leaving positively charged holes in the valence band (VB). By selecting a coating material with a sufficiently large energy barrier between the energy bands of the coating and the luminescent material, the charge carrying electrons and holes are confined to the luminescent material. This increases the efficiency of electron-hole recombination, leading to an increase in the intensity of the emissions.

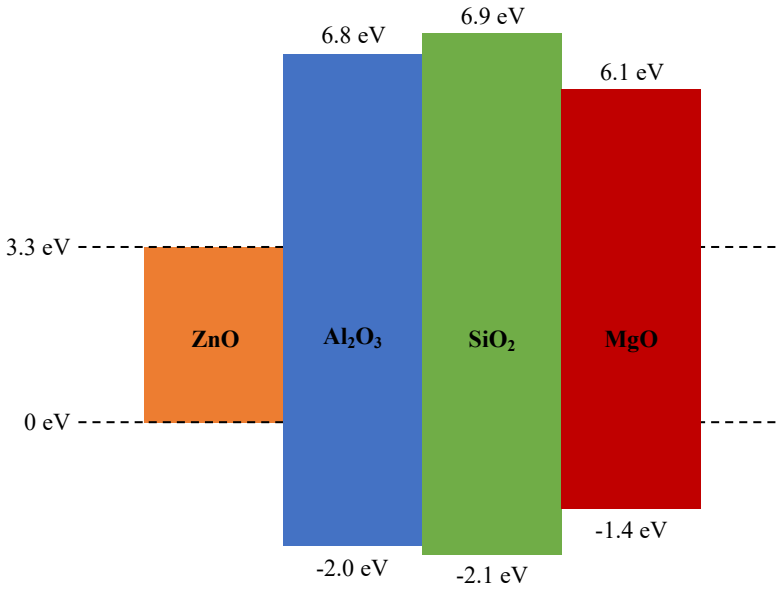

Figure 4.2 Alignments of the conduction and valence bands of the ZnO films and the coatings utilized in this research.[3] All of the coatings used formed a type 1 junction with the underlying ZnO films.

4.3 Aluminum Oxide (Al_2O_3)

Aluminum oxide (Al_2O_3) , also known as alumina, is an abundant material that is inexpensive, stable and typically grows in a corundum crystal structure. It is a widely used ceramic that is known for its stability at high temperatures and it extreme durability. Al_2O_3 has a bandgap of 8.8 eV and an average bond energy of -415.9 kJ/mol.[4,5] In this work, Al_2O_3 coatings were deposited via reactive RF sputtering using a locally fabricated target. The Al target material was sourced from Alfa Aesar, and had a purity of 99.8%. Oxygen was introduced into the growth chamber, as discussed in Chapter 2.2.3 and 2.2.7, to achieve the Al_2O_3 coating. RF sputtering was chosen for the Al_2O_3 coatings due to the rapid deposition rate of Al compared to the other coatings and to maintain consistency with as many variables as possible.

4.4 Silicon Dioxide (SiO_2)

Silicon dioxide (SiO_2), or quartz, is an extremely durable, abundant material that is also inexpensive and environmentally friendly. SiO_2 typically grows in a hexagonal structure. It is used in a wide variety of products such as windows and countertops. SiO_2 has a bandgap of 9.0 eV and an average bond energy of -455.5 kJ/mol.[4,6] In this work, SiO_2 coatings were deposited via RF sputtering reactively using a p-type, B-doped, Si wafer purchased from MTI. Oxygen was introduced into the growth chamber, as discussed in Chapter 2.2.3 and 2.2.7, to achieve the SiO_2 coating. Prior to deposition of this material, extreme caution was taken to slowly ramp the RF power up to the deposition power of 40 W to prevent thermal shock to the silicon wafer used in deposition.

4.5 Magnesium Oxide (MgO)

Magnesium oxide (MgO) is an abundant material that is environmentally friendly and is commonly found in antacids used for heartburn relief. MgO has a bandgap of 7.5 eV and an average bond energy of -593.3 kJ/mol.[4,7] In this work, MgO coatings were deposited via reactive RF sputtering using a locally fabricated target. The Mg target material was sourced from Alfa Aesar, and had a purity of 99.9%. Oxygen was introduced into the growth chamber, as discussed in Chapter 2.2.3 and 2.2.7, to achieve the MgO coating.

4.6 References

1. W. Hu and J. Yang, J. Mater. Chem. C. **5**, 47 (2017).
2. A. Amany, D. Wang, J. Wang, Z. Zeng, S. Jiao, C. Hao, Y. Zhao, Y. Xie, S. Gao, S. Ni, C. Luan, A. Alarabi, J. Taban, and L. Zhao, Journal of Alloys and Compounds **776**, 111 (2019).
3. S. Xu, R. Jacobs, H.M. Nguyễn, S. Hao, M. Mahanthappa, C. Wolverton, and D. Morgan J. Mater. Chem. A. **3**, 1039 (2015).
4. CRC Handbook of Chemistry and Physics, ed. R. C. Weast (CRC PRESS, INC., Boca Raton, Florida, 1980) 69th ed., p. D-51, D-73, D-83.
5. R.H. French, R.L. Coble, R.V. Kasowski, and F.S. Ohuchi, Physica B+C **1-2**, 47 (1988).
6. T.H. DiStefano and D.E. Eastman, Solid State Comm. **9**, 2259 (1971).
7. P.G. Mather, J.C. Read, and R.A. Buhrman, Phys. Rev. B **73**, 205412 (2006).

Chapter 5: ZnO Thin Film UV-PL Intensity Enhancement

5.1 Overview

In order to improve the UV-PL intensity of ZnO thin films, coatings of various materials were deposited onto the surface of the films. A process was developed that produced the greatest intensity enhancement for all of the materials. The resulting improvements in the PL intensity due to the different coating materials was analyzed to determine if a relationship between the material properties and the intensity improvement could be determined. Once this relationship was established, a mechanism that could explain this relationship was determined. In this chapter, the process that was developed to maximize the intensity, the results of this research and the underlying mechanism to explain the intensity enhancement are discussed.

5.2 Experimental Process

The typical steps of the experimental approach are described here. After deposition the as-grown films were analyzed via optical spectroscopy to establish reference spectra. Then a portion of the samples were annealed, typically at 900º C for 60 minutes in an Ar atmosphere. These samples were characterized again in order to determine the effect of annealing on the optical properties. The as-grown and annealed samples were returned to the growth chamber for coating deposition. Finally, the coated films were analyzed via optical spectroscopy to determine the impact of the coating on the optical properties of the films.

5.3 Experimental Results and Discussion

To achieve the primary goal of this research, which was to determine which coating material that produced the greatest improvement in photoluminescent intensity, ZnO thin films were grown, annealed at 900º C, coated and characterized as previously discussed. Al_2O_3, SiO_2 and MgO coatings were selected based on the criteria listed in Chapter 4. As can be seen in Figure 5.1, the ~ 3.28 eV UV-PL of the ZnO coated samples exhibit an enhancement relative to the uncoated ones. The intensity of the luminescence increased by ~ 52, ~ 15, and ~ 4 times, for the MgO, SiO_2, and Al_2O_3 coated samples, respectively.

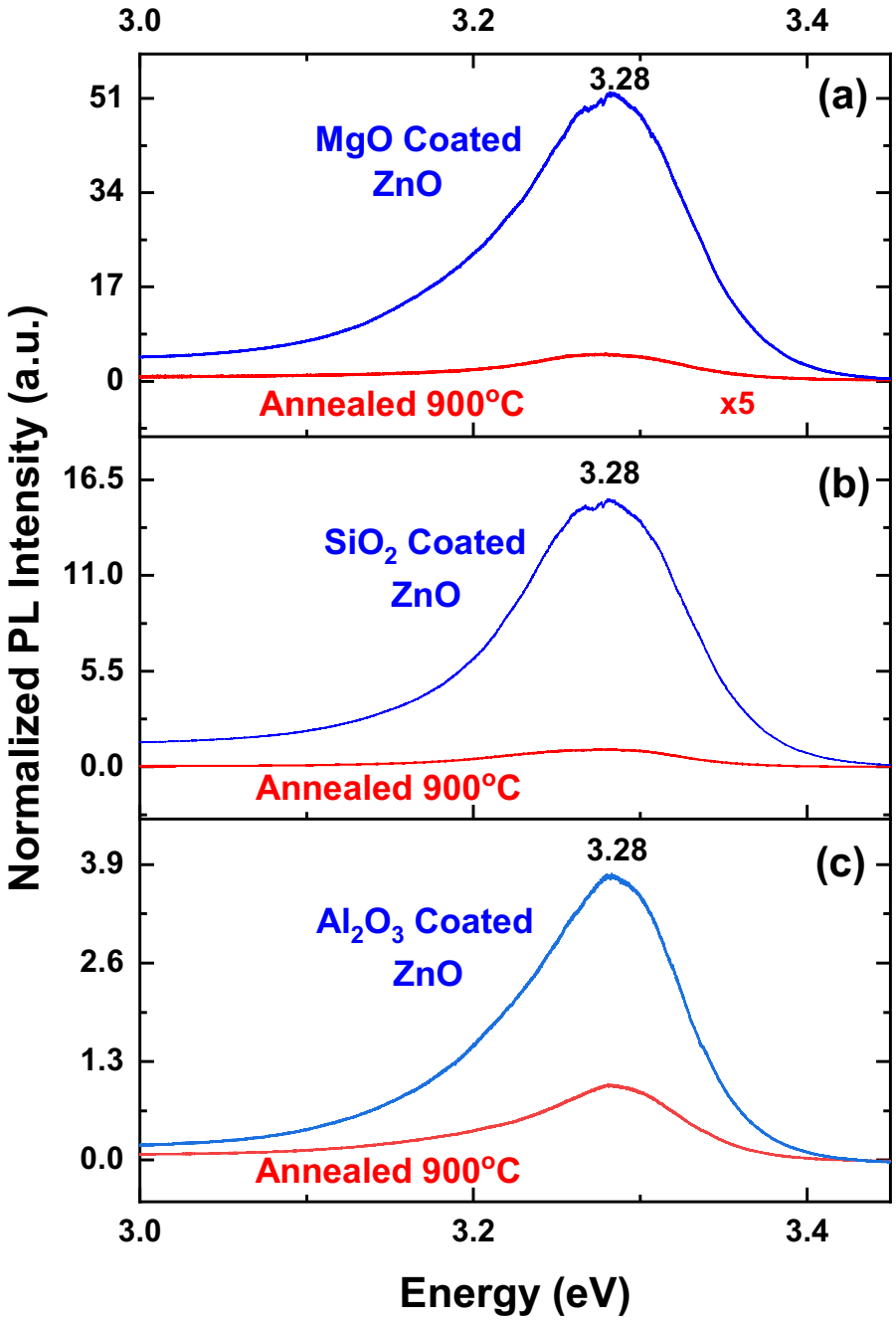

Figure 5.1 For this study, the as-grown films were annealed at 900º C (referred to in the figure as Annealed 900º C), and then coated. UV-PL spectra of ZnO coated with (a) MgO, (b) SiO_2 and (c) Al_2O_3, with intensity improvements of ~ 52x, ~ 15x and ~ 4x, respectively, relative to the uncoated films (lower spectra).

Transmission spectra were collected to determine if significant sharpening of the band edge spectra occurred, which would indicate a significant improvement of the coated film over the uncoated one. These measurements were also performed to ensure that the deposited coatings were non-reflective. The transmission spectra for each of the coating materials are shown in Figure 5.2. Since little change was observed between the uncoated and the coated films, the spectra indicate that the defects treated by the coatings were indeed isolated to the surface, as expected. It also shows that a reflective surface is not present on the post-coating films, so that is not the source of the intensity improvement observed.

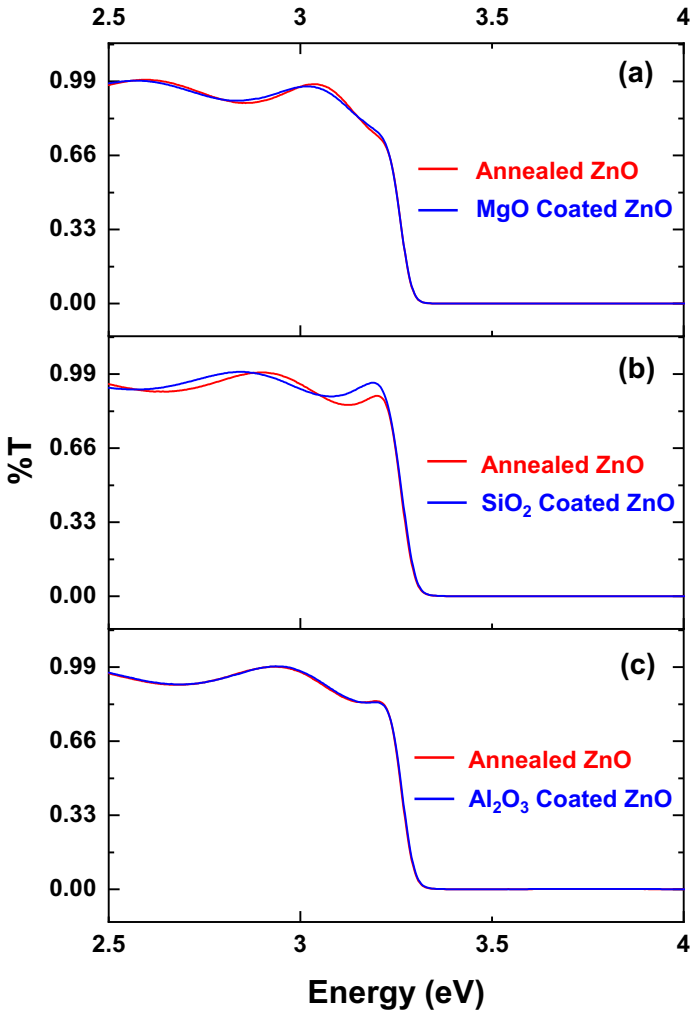

Figure 5.2 Transmission spectra of ZnO coated with (a) MgO, (b) SiO_2 and (c) Al_2O_3. The minimal differences in the spectra between the coated and the uncoated film indicate that the source of the intensity enhancement is due to surface defect treatment.

In an attempt to determine a possible relation between the intensity improvement produced by the coating process and the coating material used, the average bond energy of each of the materials was analyzed. These values and the bandgaps for each of the coating materials are shown in Table 5.1. Bandgap values were taken from literature and the bond energies were determined from the formation energies, ΔH^o_f, of Al_2O_3, SiO_2, MgO, and ZnO,[2] divided by the number of bonds in the corresponding molecule.[3]

Table 5.1 Relevant properties of the coating materials used. A strong linear correlation between the average bond energy of the coating and the UV-PL intensity improvement of the films was observed, as shown in Figure 5.3. ZnO properties are also included.

Material	Bonds per Molecule	Average Bond Energy (kJ/mol)	Bandgap (eV)
Al_2O_3	4	-415.9	8.8
SiO_2	2	-455.5	9.0
MgO	1	-593.3	7.5
ZnO	1	-348.3	3.3

Analysis of these values revealed a linear correlation between the average bond energy of the coating material and the observed UV-PL intensity enhancement, as shown in Figure 5.3. A discussion of this linear correlation follows in terms of surface contaminants, the sputtering environment, and the coating bond energies.

It is a well-known phenomenon that ZnO surfaces are susceptible to adsorption of environmental contaminants. These adsorbates can act as non-radiative centers, resulting in diminished UV-PL.[4-6] For example, Zn-terminated surfaces are prone to adsorption of OH-groups, while oxygen terminated surfaces can adsorb H^+.

As previously discussed in Chapter 5.2, the coating process in the sputtering chamber starts with heating the annealed ZnO samples to 250º C under vacuum $<10^{-4}$ torr for about one hour. These conditions are sufficient to remove most of the adsorbed surface contaminants.[6] However, it is expected that some of the H^+ and OH-groups are still present in the growth chamber, and can re-adsorb onto the ZnO surfaces.

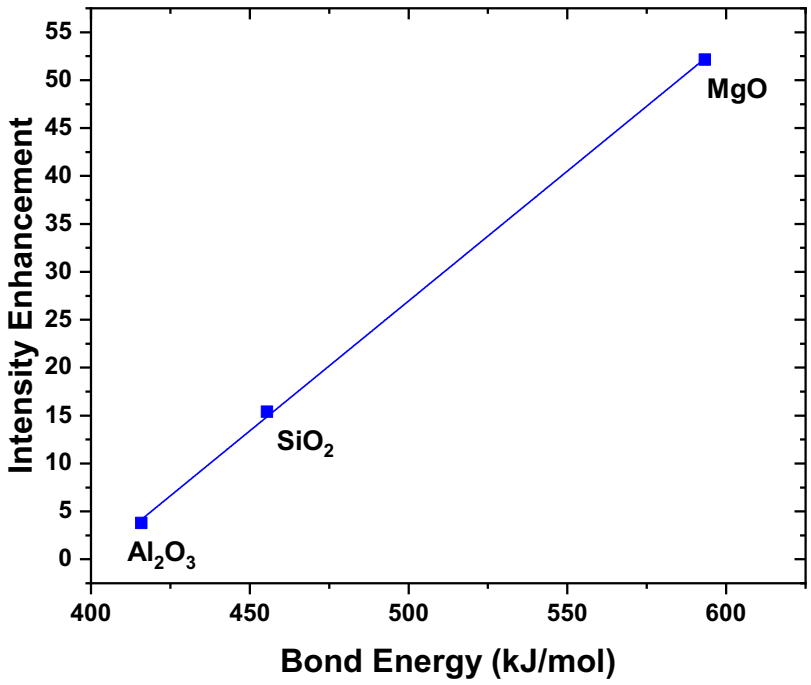

Figure 5.3 The linear correlation between the UV-PL intensity enhancement and the bond energy of the coating material. Among the three, MgO seems to be the material of choice for the coating of ZnO.

Removal of surface contaminants from the Zn- or O-terminated crystal faces should result in the presence of dangling bonds. Once the oxygen-rich plasma is initiated, the O^{2-} species can passivate the dangling bonds on the Zn-terminated surfaces. These newly O-terminated surfaces can now bond to the Al^{3+}, Si^{4+}, or Mg^{2+} ions being sputtered from the target in the final stage of the coating process. This process is depicted in Figure 5.4.

The observed direct correlation between the bond strength of the coating materials and the enhancement of PL intensity indicates that the coating materials are likely competing with other on-going surface processes, such as surface reconstruction and re-adsorption of the residual contaminants such as OH-groups. The stronger the bond energy, the higher the probability is of passivating the surface.

One process that occurs during sputtering is gas phase nucleation of the coating molecules.[7] This process produces polar molecules in the plasma for each of the coating molecules studied. These molecules can bond with the previously discussed dangling bond sites on the surface, whether they are O-terminated or Zn-terminated. Once again, the direct

correlation between bond energy and PL intensity enhancement can be explained by the bond affinity of the coating material and the O^{2-} ions in the plasma. This process is depicted in Figure 5.5.

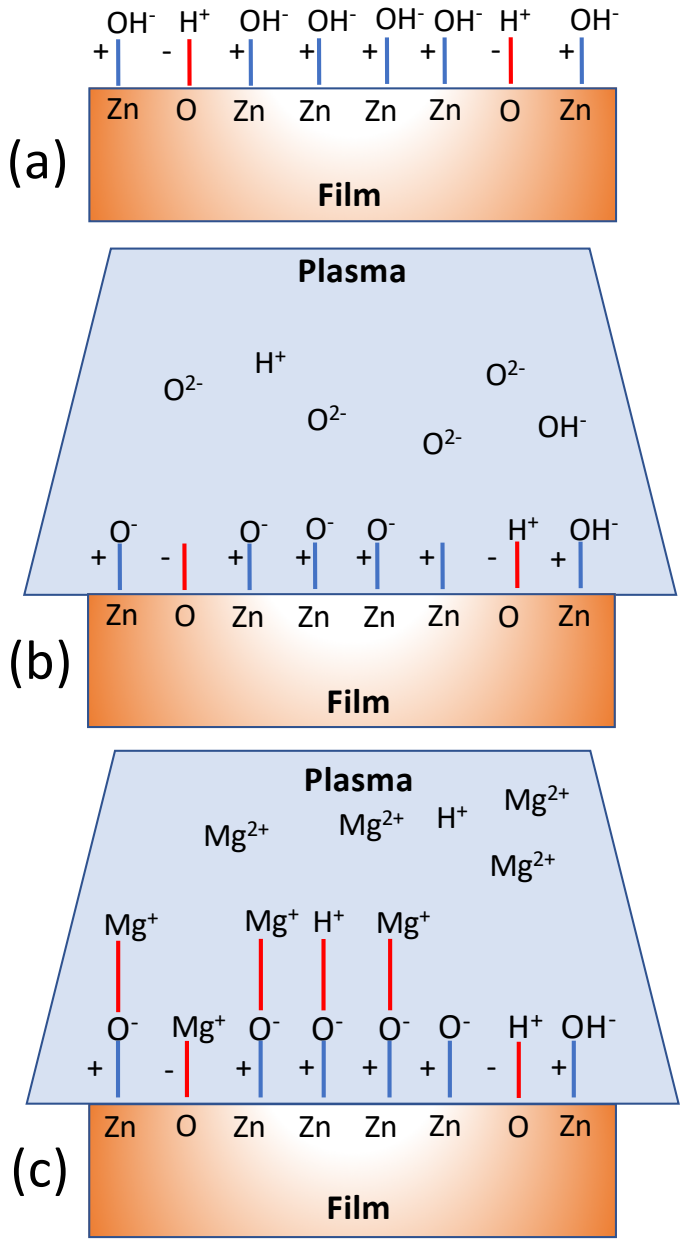

Figure 5.4 ZnO thin films at various stages of MgO coating. (a) Films adsorb contaminants from the environment. (b) Contaminants are removed via surface heating under vacuum, leaving dangling bonds available for bonding with O^{2-} ions or residual contaminants such as OH-groups. (c) Coating material competes with contaminants to bond to O^{2-} dangling bonds.

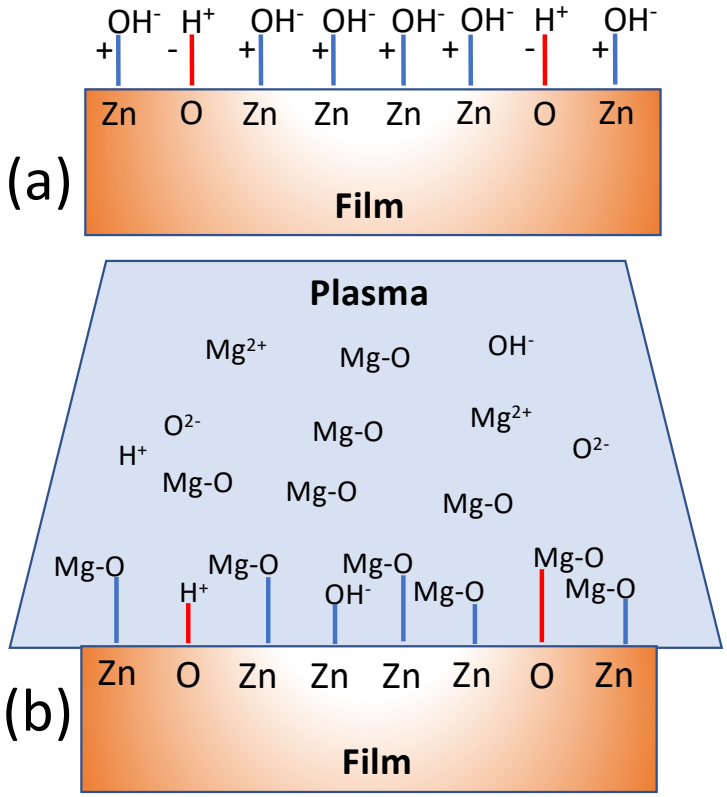

Figure 5.5 Gas phase nucleation during the MgO coating process. (a) Films adsorb contaminants from the environment. (b) Contaminants are removed via surface heating under vacuum, while O^{2-} and Mg^{2+} ions bond in the plasma prior to reaching surface. MgO molecules compete with residual contaminants for bonding to either Zn^{+} or O^{-} dangling bonds at the surface.

In this case, oxides with a greater bond energy will bond more readily in the plasma prior to reaching the ZnO surface. This will result in a greater number of coating molecules passivating the dangling bonds, thus preventing the re-adsorption of residual contaminants.

It would be expected that if the coating removes most of the non-radiative centers, the correlation presented in Figure 5.3 would follow what is commonly referred to as a "saturation curve". This relation was not observed in our work, indicating that only a portion of the defects were treated by the coatings technique. Future work will address this issue and investigate additional potential coating materials.

5.4 ZnO - Coating Interface Stress Analysis

The difference in the lattice parameters of the ZnO film and the deposited coating material can cause stress along the interface of the two dissimilar materials. The effect of the coating on the stress state of the ZnO film may be analyzed via the shift of the Raman frequency, as this method is highly sensitive to induced compressive or tensile stress. MgO coated ZnO films were analyzed for the presence of stress along this interface. Raman spectra of the ZnO LO-phonon mode of a bare film and a coated one are presented in Figure 5.6. As can be seen in the figure, coating with MgO did not result in a frequency shift, implying that stress induced by the coating is negligible.

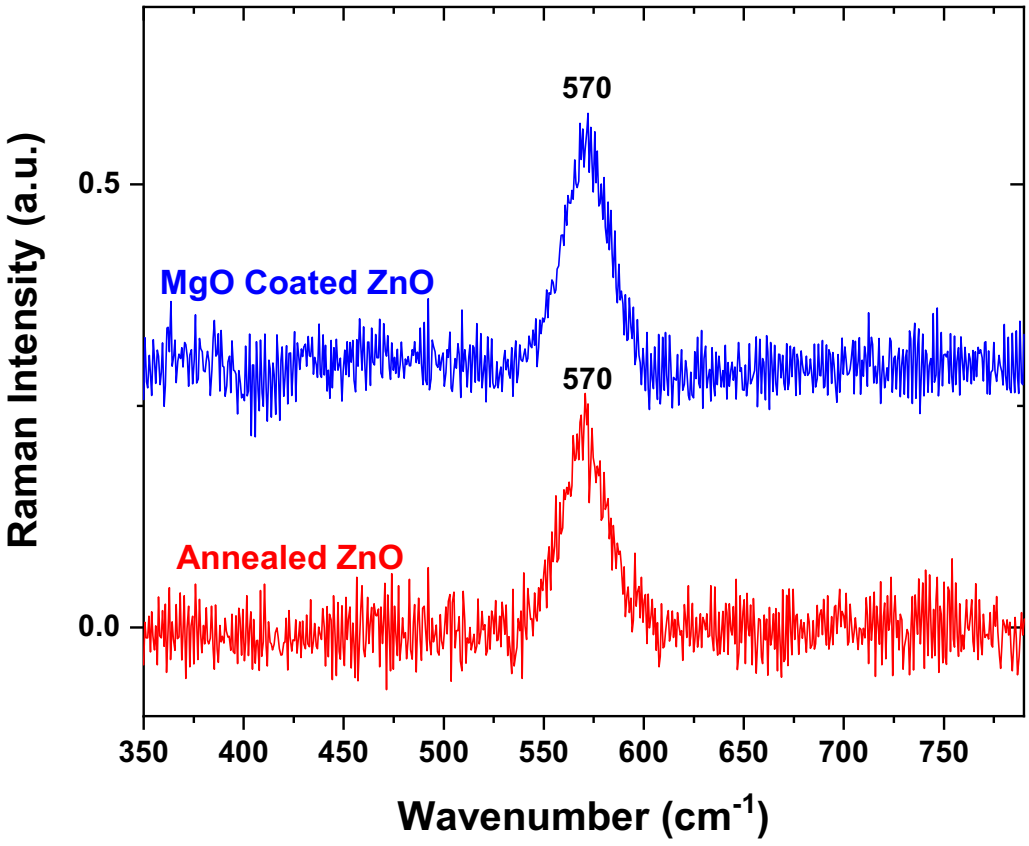

Figure 5.6 Raman spectra of uncoated ZnO and MgO coated ZnO. The LO-mode of both samples is at 570 cm^{-1}. The absence of a shift in the LO-mode of the ZnO after coating with MgO indicates that the stress induced on the underlying ZnO by the MgO coating is negligible.

5.5 Effects of Annealing on Coated ZnO Films

An additional study was conducted on ZnO films coated with Al_2O_3 to determine if annealing of the coating would produce additional intensity enhancement when compared to a non-annealed, coated sample that was previously studied. In this study, one ZnO film was coated with Al_2O_3 using a 250º C substrate temperature. The coated sample was then subjected to a 500º C post-deposition annealing treatment for 60 minutes in an Ar environment. A second ZnO sample received an Al_2O_3 coating under the same conditions, except that the substrate temperature was 500º C during growth. This temperature was held for ~ 60 minutes, with the coating deposition occurring during the final ~ 2 minutes. The second sample did not undergo a post-deposition annealing. The impact of the different processes is shown in Figure 5.7.

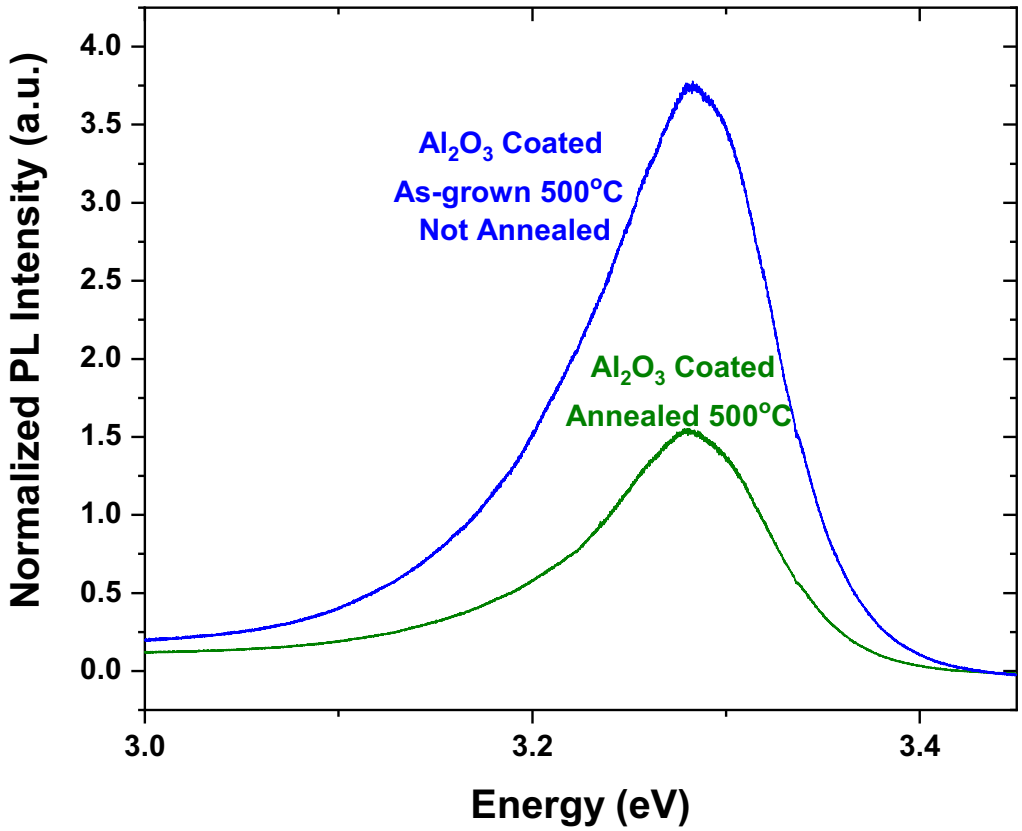

Figure 5.7 PL spectra of Al_2O_3 coated ZnO. Lower trace is the PL of the annealed sample, and the upper trace is that of a non-annealed sample.

Based on the improvements in crystal quality and material performance observed after annealing ZnO, which will be discussed later, it was expected that annealing of the coatings would improve the quality of the coating, and by extension improve the intensity of the UV-PL. As can be seen Figure 5.7, after annealing, the UV-PL intensity of the coated sample exhibits ~ 60% decrease relative to the of the non-annealed, coated sample. An initial explanation for this phenomenon is that the annealing process disrupts the ZnO-coating interface, allowing contaminants to re-adsorb, and reconstruction to take place on the ZnO surface. Shifts in the PL or Raman spectra of these samples were not observed, so alloying of the coating and ZnO films after annealing is not a likely cause for the decrease in UV-PL intensity. This is an initial assessment of this mechanism, and it is expected that future work will yield a more complete understanding of this phenomenon.

5.6 Effect of Annealing on ZnO Films Prior to Coating: Native Defects

Many studies have previously shown that as-grown ZnO films contain native defects that can lower the UV emission efficiency, and create luminescence centers in the visible part of the spectrum. Moreover, post-growth annealing treatments were found to be an effective approach to reduce the density of various native defects in the bulk of the films, resulting in enhanced UV light emission in ZnO films.[8-10] In order to investigate the effect of native defects on the ZnO PL, we performed an annealing study in an argon environment. The UV-PL of an as-grown ZnO film, ZnO annealed at 600º C, and ZnO annealed and then coated with MgO is shown in Figure 5.8. The peak intensity of the film annealed at 600º C had an ~ 8-fold improvement relative to the as-grown film. Coating of this film after annealing produced a ~ 70-fold UV-PL enhancement over the as-grown film.

In order to understand the impact of the annealing temperature, an additional annealing study at a higher temperature was performed. The UV-PL of an as-grown ZnO film and a film annealed at 900º C are presented in Figure 5.9. Also included in the figure is the spectrum of the 900º C annealed ZnO film that was coated with MgO.

The peak intensity of the film annealed at 900º C had a ~ 59-fold improvement relative to the as-grown film. Coating of this film after annealing produced a ~ 3070-fold UV-PL enhancement over the as-grown film. When compared to the results shown in Figure 5.8, it is clear that annealing at 900º C prior to coating, is more beneficial to the enhancement

process than annealing at 600º C prior to coating. A previous study indicated that significant improvement in the film's morphology occurs at annealing ~ 900º C [8], which is conducive to a better coverage of the coating.

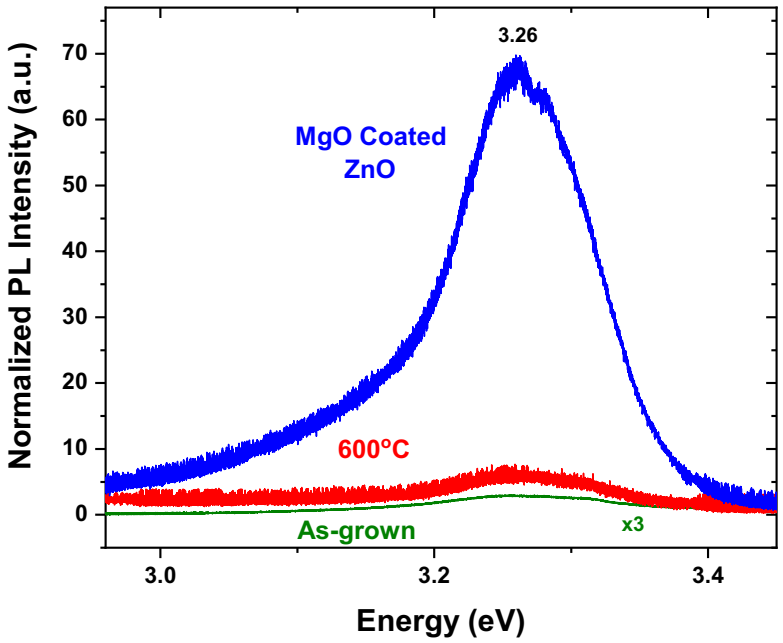

Figure 5.8 PL spectra of as-grown and 600° C annealed ZnO films. The upper spectrum is the PL of the 600º C annealed film with a MgO coating. Intensity values were normalized to the as-grown spectra and the peak values are as follows: as-grown ZnO = 1, 600° C annealed ZnO = 8, and MgO coated ZnO = 70.

Further analysis of the data presented in Figure 5.9, shows that annealing alone at 900º C is responsible for ~ 2% of the total UV-PL intensity enhancement, while the coating treatment contributes the remaining ~ 98% of the enhancement. This led to the conclusion that surface defects in these nano-crystalline films are more detrimental to UV-PL intensity than defects in the bulk of the film.

Several groups have previously addressed the issue of native defects in relation to the UV-PL of ZnO films and nanostructures.[8-10] To get an insight into the impact of native defects on the UV-PL intensity of the sputtered ZnO films, luminescence experiments that include the visible part the spectrum were performed. Figure 5.10 shows the PL of the as-grown ZnO film, while Figure 5.11 presents the PL after the annealing treatment at 900º C.

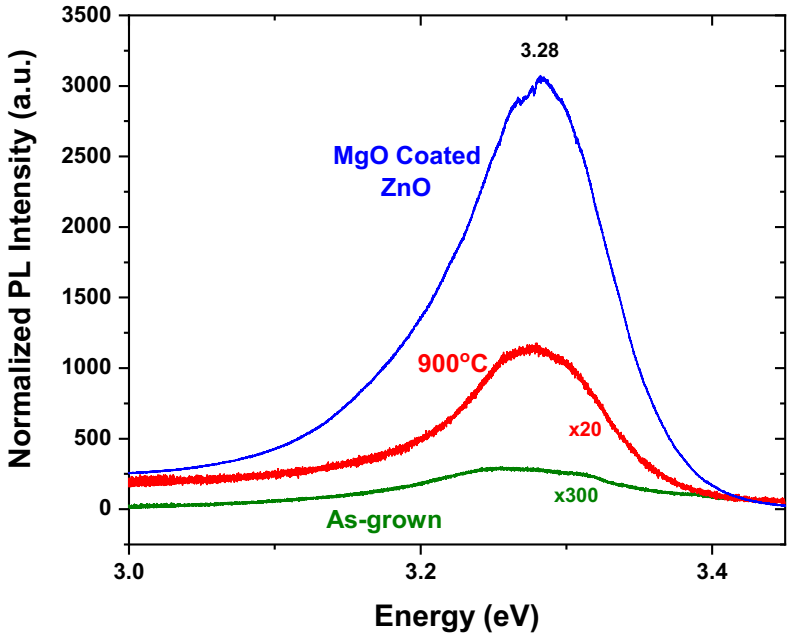

Figure 5.9 PL spectra of as-grown and 900º C annealed ZnO films. The upper spectrum is the PL of the 900º C annealed film with a MgO coating. Intensity values were normalized to the as-grown spectrum and the peak values are as follows: as-grown ZnO = 1, 900º C annealed ZnO = 59, and MgO coated ZnO = 3071.

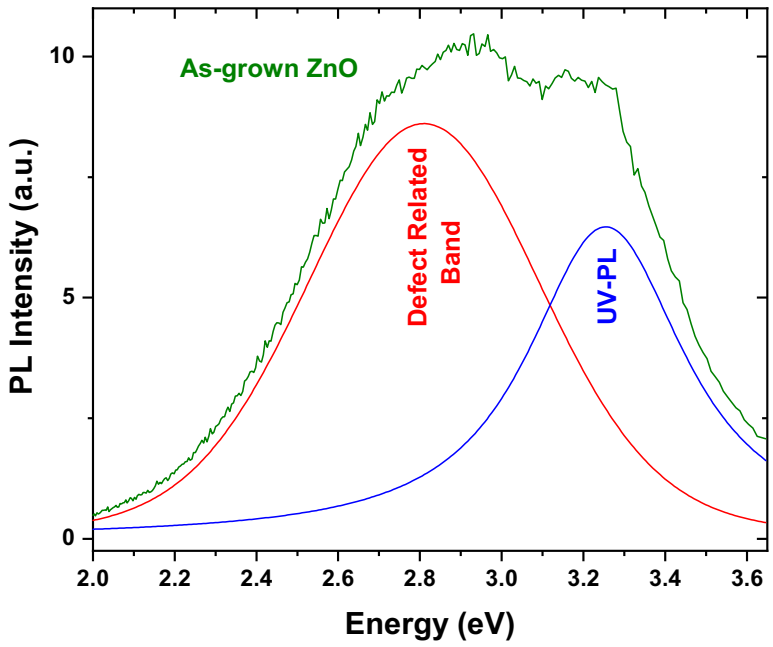

Figure 5.10 PL spectrum of as-grown ZnO film indicates the presence of band edge UV and native defect related visible emissions.

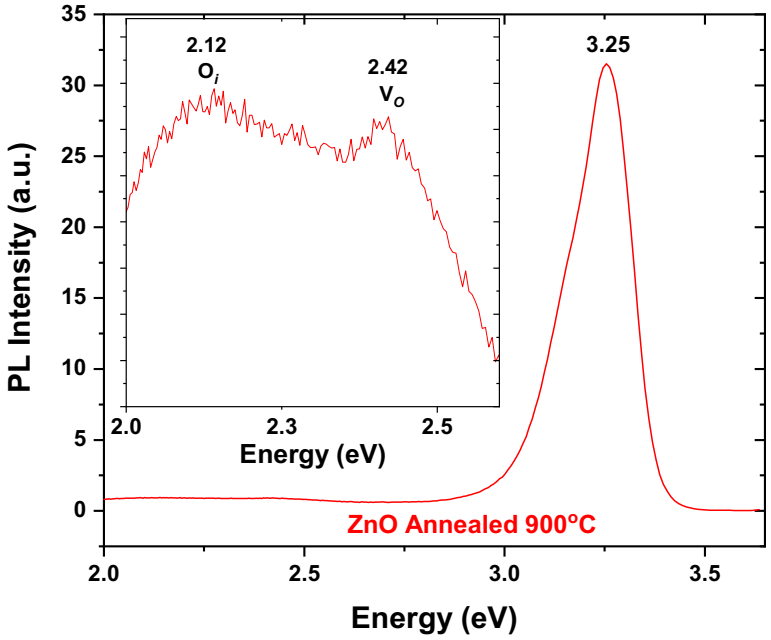

Figure 5.11 PL spectrum of ZnO film annealed at 900° C under Ar. The visible emissions commonly attributed to native defects are mostly quenched, while the UV-PL is significantly enhanced. The inset is the zoomed spectrum at the visible range showing luminescence peaks at 2.12 eV and 2.42 eV attributed to residuals of oxygen interstitials and oxygen vacancies, respectively.

The spectrum of the as-grown film consists of the UV-PL at ~ 3.25 eV and a broad visible band. The broad visible band has been extensively studied and shown to be a convolution of PL emissions originating from several types of native defects such as oxygen and Zn interstitials, and oxygen and Zn vacancies.[8,11-14] Previous work has shown that the growth environment in the sputtering chamber is conducive to the incorporation of Zn interstitials with an emission peak ~ 2.8 eV, as shown in Figure 5.10.[8] These types of native defects are highly unstable[15] and can be annealed out at low temperatures. On the other hand, oxygen vacancies and oxygen interstitials are more stable defects in ZnO and residuals are still present even after annealing at high temperatures, as can be inferred from the inset in Figure 5.11.

Although still debatable, the ~ 2.12 eV and the ~ 2.42 eV PL emission, shown in the inset of Figure 5.11, are commonly assigned to oxygen interstitials and oxygen vacancies, respectively.[11,12] The main point of interest, presented in Figure 5.11, is that after the

annealing treatment, the intensity of the visible band significantly diminished, while that of the UV-PL showed an improvement. The results presented in Figures 5.10, and 5.11 point to the role of native defects in the PL enhancement process.

5.7 Optimal Process for Intensity Improvement

In the course of our research on this subject, and based on the research discussed in the previous section, an optimal process for improving the intensity of the UV-PL in ZnO thin films was determined. This process requires high-temperature annealing of the ZnO films prior to coating in order to eliminate native defects. Moreover, there is no need to anneal a coated sample. This step resulted in the weakening of the PL intensity, which is attributed to a degradation of the ZnO/coating interface. Possible degradation is due to the incorporation of environmental contaminants. Figure 5.12 describes the expected performance of the ZnO films based on various steps that were taken during this research.

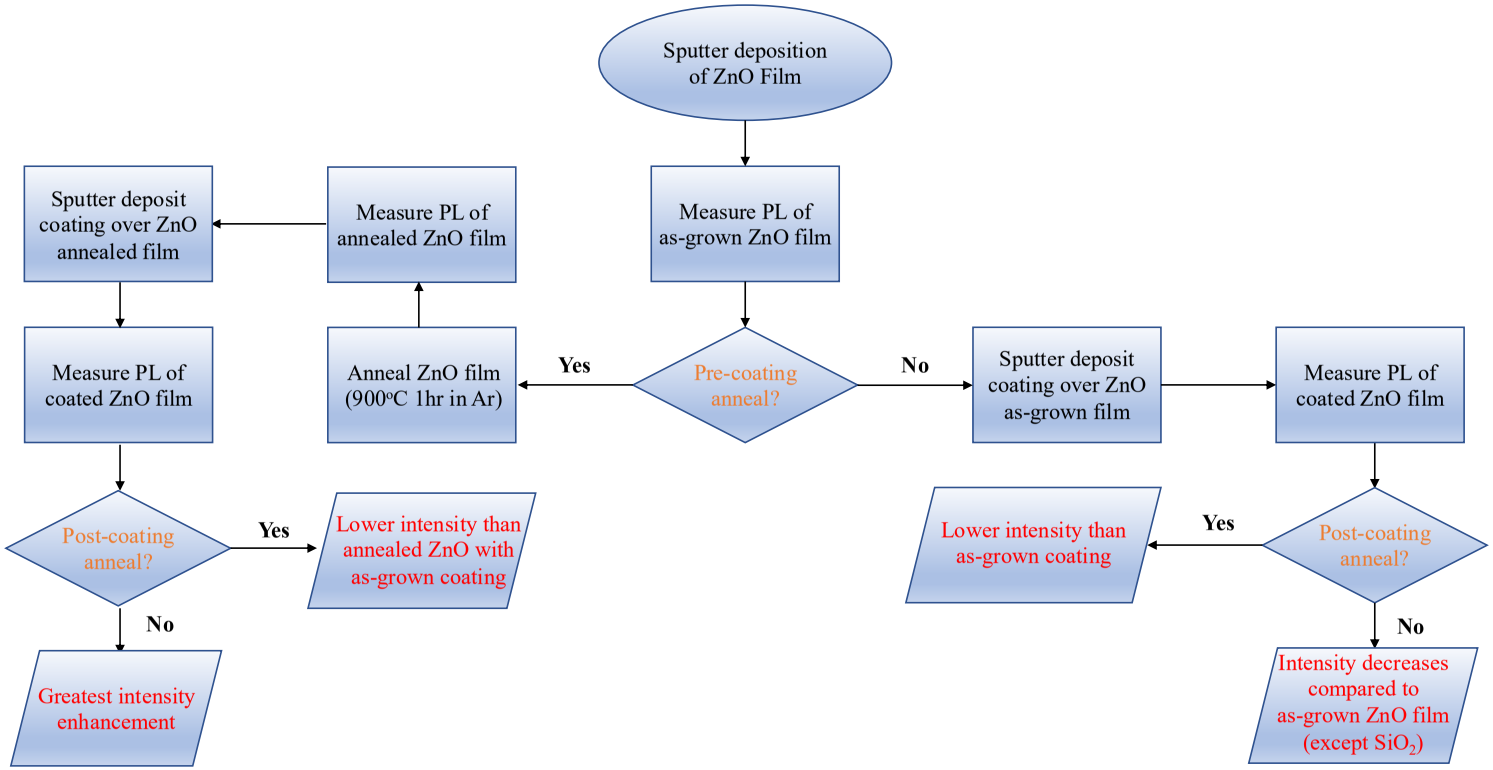

Figure 5.12 Flowchart showing various expected outcomes based on possible steps taken during this research. The optimal method for achieving the maximum UV-PL intensity enhancement is to anneal the ZnO film prior to coating deposition. Post-deposition annealing of the coatings caused the UV-PL intensity to diminish.

5.8 Summary

In this research, two approaches for the enhancement of the UV band edge luminescence in ZnO films were studied: one that used surface coating, and another that employed annealing in a non-oxidizing environment of Ar gas. This research led to the following conclusions:

- Deposition of a MgO coating on an annealed ZnO film produced a 52-fold increase in the UV-PL intensity compared to an uncoated, annealed ZnO film.
- Al_2O_3, SiO_2 and MgO coatings were studied, and MgO is the most effective coating material due to its high bond energy.
- A strong linear relation between the PL intensity improvement and the average bond energy of the coating material exists.
- The PL intensity enhancement is explained by competing mechanisms that passivate surface traps such as OH-groups, which can lead to lower UV-PL intensity.
- A process combining both annealing and coating to produce the greatest UV-PL enhancement was developed. Annealing at 900º C, prior to the deposition of the coating, optimized the performance of the coating material.
- The presence of surface defects in these films have a greater detrimental impact on the UV-PL intensity than bulk native-defects.
- Annealing the films after coating deposition leads to diminished UV-PL intensity.

Future work on this topic will involve additional coating and luminescent materials, along with studies of a wider range of annealing temperatures for the ZnO films prior to coating. These topics will be discussed in greater detail in the following chapter.

5.9 References

1. D.L. Smith, *Thin-Film Deposition: Principles and Practice*, 2nd ed. (McGraw-Hil, New York, 1995) pp 421-440.
2. CRC Handbook of Chemistry and Physics, ed. R. C. Weast (CRC PRESS, INC., Boca Raton, Florida, 1980) 69th ed., p. D-51, D-73, D-83.
3. I.N. Lavine, *Physical Chemistry*, 6th ed. (McGraw-Hill, New York, 2008), pp. 166-167.
4. H. Idriss and M.A. Barteau, J. Phys. Chem. **96**, 3382 (1992).
5. W.Z. Liu, H.Y. Xu, J.G. Ma, C.Y. Liu, Y.X. Liu, and Y.C. Liu, Appl. Phys. Lett. **100**, 203101 (2012).
6. C. Chen, H. He, Y. Lu, K. Wu, and Z. Ye, ACS Appl. Mater. Interfaces **5**, 6354 (2013).
7. M.C. Barnes, A.R. Gerson, S. Kumar, and N.-M Hwang, Thin Solid Films **446**, 29 (2004).
8. D. Thapa, J. Huso, J.L. Morrison, C.D. Corolewski, M.D. McCluskey, and L. Bergman, Opt. Mater. **58**, 382 (2016).
9. V.V. Khomyak, M.M. Slyotov, I.I. Shtepliuk, G.V. Lashkarev, O.M. Slyotov, P.D. Marianchuk, and V.V. Kosolovsky, J. Phys. Chem. Solids **74**, 291 (2013).
10. L. Lin, J. Liu, J. Lv, S. Shen, X. Wu, D. Wu, Y. Qu, W. Zheng, and F. Lai, J. Alloys Compd. **695**, 1523 (2017).
11. K. Vanheusden, C.H. Seager, W.L. Warren, D.R. Tallant, and J.A. Voigt, Applied Physics Letters **68**, 403 (1996).
12. C. Chandrinou, N. Boukos, C. Stogios, and A. Travlos, Microelectron. J. **40**, 296 (2009).
13. J. Čížek, J. Valenta, P. Hruška, O. Melikhova, I. Procházka, M. Novotný, and J. Bulíř, Appl. Phys. Lett. **106**, 251902 (2015).
14. H. Zeng, G. Duan, Y. Li, S. Yang, X. Xu, and W. Cai, Adv. Funct. Mater. **20**, 561 (2010).
15. A. Janotti and C.G. Van de Walle, Rep. Prog. Phys. **72**, 126501 (2009).

Chapter 6: Coating Efficiency: Time Evolution Study of Environmental Exposure

6.1 Overview

This chapter focuses on the time evolution properties of the coating. Specifically, the PL of the coated ZnO was studied as a function of exposure time to the environment in order to gain an insight into their resistance to recontamination. The samples were exposed to an atmospheric environment for up to 242 days, and their optical and material properties were periodically explored.

6.2 Degradation of Coating Effectiveness

For this research to be applied to device technologies, a crucial consideration that must be taken into account is the effectiveness of the coatings over long periods of time in a typical environment the material might be used in. During this research, three ZnO films, one coated with SiO_2, another coated with MgO, and a third uncoated film were stored in air and periodically retested via PL and Raman spectroscopy to observe changes in the bandgaps and intensities over a period of ~ 11 months. The films did not exhibit an energy shift or change in the Raman intensity for either sample over this period. The PL spectrum of the SiO_2 coated film and the uncoated film also remained constant throughout the testing period. The PL spectra of the SiO_2 coated film is shown in Figure 6.1.

The PL spectrum of the ZnO films coated with MgO are shown in Figure 6.2. The intensity of the UV-PL emissions diminished by ~ 65% after exposure to the air for 294 days, resulting in a UV-PL intensity that is comparable to that of the SiO_2 coated sample. To further investigate the effect of the air environment on the MgO and SiO_2 coatings SEM imaging both samples was performed.

During a 242 day exposure to air, the MgO coatings formed dark regions with diameters up to ~ 40 μm. Images of the MgO coatings before and after the formation of the dark regions are shown in Figure 6.3(a) and (c). In order to determine if there were compositional differences between the dark and light regions, a backscatter image of the

MgO coated sample after formation of the dark regions was taken, and is shown in Figure 6.3(d).

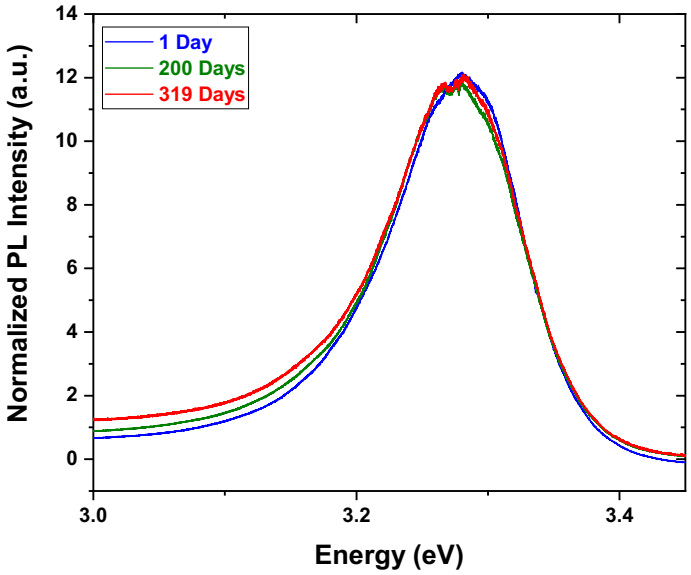

Figure 6.1 PL spectra of a ZnO film with a SiO_2 coating; 1, 200, and 319 days after the coating was deposited. The intensity and energy of the UV-PL in these samples remained consistent throughout the testing period, indicating that the surrounding environment has little impact on the effectiveness of the SiO_2 coating.

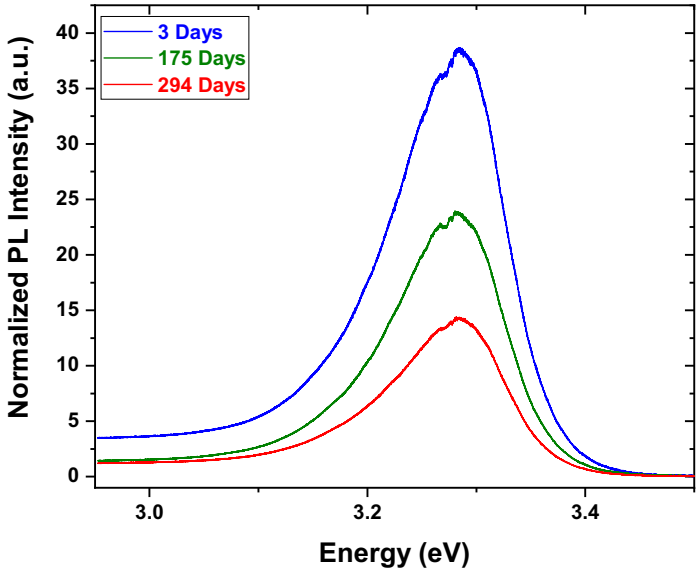

Figure 6.2 PL spectra of ZnO films coated with a MgO coating; 3, 175, and 294 days after coating deposition. Significant degradation of the UV-PL intensity indicates that MgO coatings are highly sensitive to exposure to air.

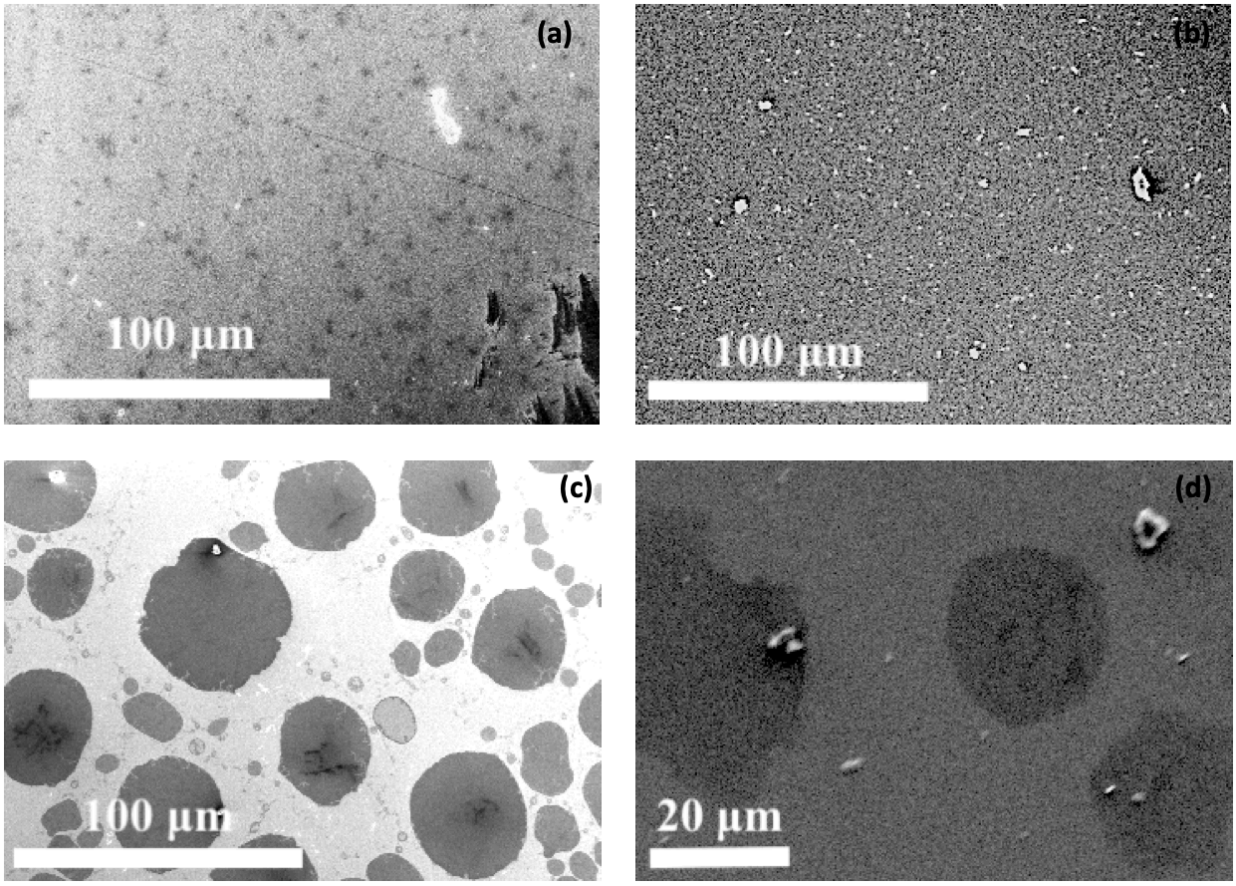

Figure 6.3 In-lens SEM images of (a) a ZnO film one day after coating with MgO, (b) a ZnO film 341 days after coating with SiO_2, and (c) a ZnO film 242 days after coating with MgO. Large dark regions formed in the MgO coated sample , while the SiO_2 coating remains uniform. (d) Backscatter image of the MgO coated ZnO film shown in (c). The contrast between the dark and light regions indicates differences in the chemical composition of the two regions.

The backscatter image, presented in Figure 6.3(d) indicates that there is a compositional difference between the dark and light regions of the coating, due to electron energy differences in the elastic scattering events that occur around atoms with different atomic numbers. Lighter regions, with higher energy backscattered electrons, indicate the presence of elements with a higher average atomic number than the darker regions.[1] Surface degradation was not observed in the SiO_2 coated sample, which is shown in Figure 6.3(b). At this time, the source of the degradation of the MgO coatings is unknown. Future work will seek to identify the origin of the coating degradation.

6.3 Summary

MgO was found to be the optimal coating material for enhancement of the UV-PL among the coatings tested, but it was also found to be subject to environmental degradation. The PL intensity diminished significantly over the course of 242 days, resulting in performance that is similar to that of the SiO_2 coated films. The SEM image gathered using an in-lens detector follows the PL result, and indicates that the MgO coating degraded over the test period, while the backscatter images indicate a compositional difference between the light and dark regions of the coating. On the other hand, the SiO_2 coating did not degrade, and its PL was not impacted by the long exposure to the environment.

6.4 References

1. M. Ohring, *Materials Science of Thin Films: Deposition and Structure*, 2nd Ed. (Academic Press, San Diego, 2002) pp 583 - 589.

Chapter 7: Ga_2O_3 Thin Film Optical Characterization

7.1 Overview

Determination of the electrical and optical properties of a material is crucial to its use in commercial applications such as optical sensors, gas sensors, and power electronics. Due to their compact scale and high surface area to volume ratios, thin films can exhibit unique characteristics that are ideal for these types of devices.[1] Basic knowledge of these properties can often be found nondestructively via optical characterization. The novel properties of Ga_2O_3, previously discussed in Chapter 1, make this material an important subject of study for realization of high performance devices.

In this work, Ga_2O_3 thin films were grown via RF sputtering with various growth parameters in an attempt to determine fundamental optical properties of this material. The films were then annealed at a temperature of 1100º C, in air and oxygen environments. Characterization of the films was performed via PL, Raman, and transmission spectroscopy. Additionally, SEM was used for surface imaging and EDS was utilized for compositional analysis. Qualitative observations of physical properties are also noted, as these observations may provide direction for more quantitative investigations in the future. A discussion of the results of the research performed is summarized in this chapter.

7.2 Impact of Growth Conditions

In this portion of the study, two different batches of samples were grown via RF sputtering. Both batches were grown using a commercial Ga_2O_3 target. The films were grown on Si<100>, Si<111>, SiO_2, and Al_2O_3 substrates heated to $\sim 400^{\circ}$ C, with an initial chamber pressure of $\sim 7.5 \times 10^{-5}$ torr and a deposition pressure of $\sim 1.2 \times 10^{-2}$ torr. The deposition power, deposition time, and the oxygen concentration of the growth environment were varied between the two sets of samples. The differences in the growth conditions along with the estimated thickness of each sample set are shown in Table 7.1. The thickness was estimated using the transmission spectra of a Ga_2O_3 sample on a SiO_2 substrate. Since annealing was required to perform optical analysis, thickness measurements were collected after annealing each sample for 3 hours at 1100º C in air.

Table 7.1 Growth condition differences between the first and second sample sets. The substrates, substrate temperatures, and chamber pressures were the same for each growth. The resulting

Sample Set	Deposition Power (W)	Deposition Time (hrs)	Ar:O_2 Ratio / Percent O_2	Thickness (nm)
1	60	5	50:1 / 2%	500
2	80	3	70:1 / 1.4%	350

After the growth of sample set 1, the samples were annealed in air 1100º C for ~ 3 hours. With annealing complete, Raman, PL and transmission characterization of the samples was performed. This set of samples will be the focus of the remainder of Chapter 7.2.

7.2.1 Raman Spectroscopy of β-Ga_2O_3 Films

Raman spectroscopy was used in this study for material and crystal structure identification. A Raman spectrum of a Ga_2O_3 film grown on Si<111>, and annealed in air, is shown in Figure 7.1. The sample was analyzed via micro-Raman using 5.1 eV laser excitation at ~ 32.5 mW. Based on the peaks observed and values from literature, the spectrum indicates that the material present in the annealed films was the monoclinic structured β-Ga_2O_3.[2] The Raman spectrum of β-Ga_2O_3 can be divided into three distinct regions, where each region originates from a unique phonon source within the crystal. The regions are shown in the crystal structure diagram in Figure 7.2. Phonons with wavenumbers less than 200 cm^{-1} originate from translational vibrations along the octahedral – tetrahedral chains. Phonons with energies of 200 – 500 cm^{-1} are from octahedral deformations, and phonons with wavenumbers from 500 – 800 cm^{-1} originate from stretching and bending of the tetrahedral regions in the crystal.[2] The Raman spectrum shown in Figure 7.1 is typical for all of the films studied. Background modes originating from the underlying substrates were removed by first collecting the spectra of a bare substrate, and then subtracting this spectrum from the spectrum of the film. Due to similarities in the Raman spectra of Ga_2O_3 and the Al_2O_3, Raman studies of films grown on Al_2O_3 substrates were frequently inconclusive and their use was discontinued in favor of SiO_2 and Si substrates.

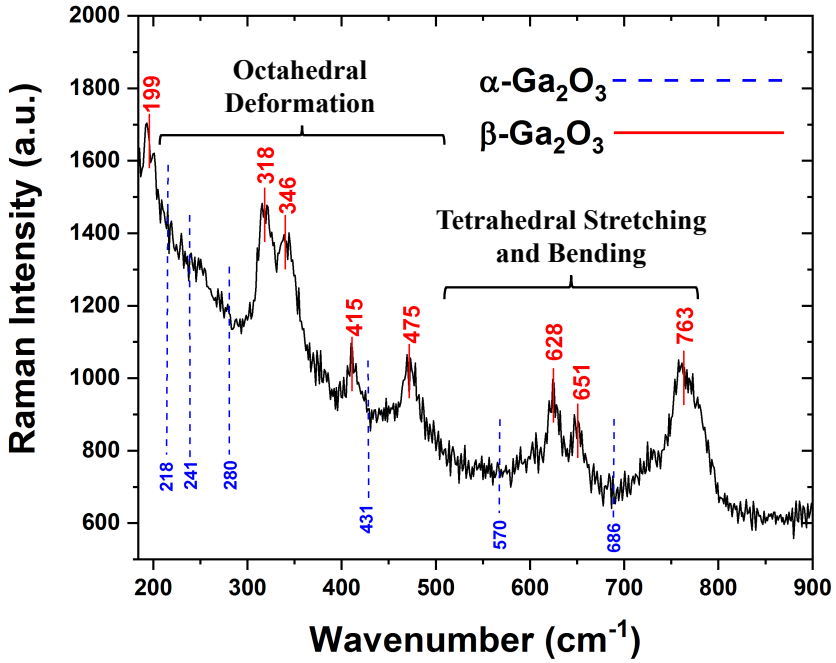

Figure 7.1 Raman spectrum of a Ga_2O_3 film grown on an Si <111> substrate. After annealing, the films were in the stable, monoclinic β-Ga_2O_3 form, which was the original goal of the growth. The Raman spectrum of β-Ga_2O_3 can be divided into three distinct regions, two of which are shown here. The dotted lines indicate the values of the α-phase Raman modes. These modes are not present, implying the purity of the β-phase.

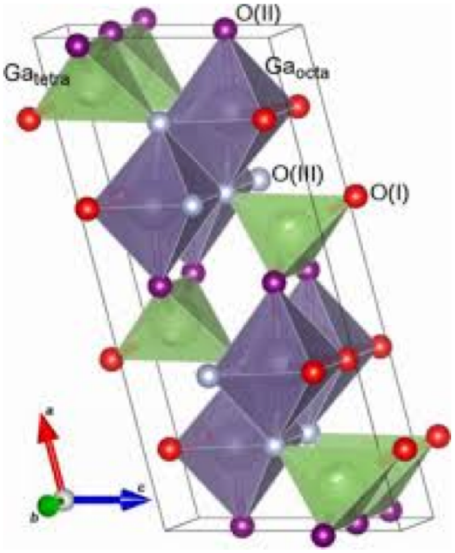

Figure 7.2 β-Ga_2O_3 crystal structure, with oxygen atoms in red, and gallium atoms in purple. Tetrahedral regions, which are the source of Raman modes from 500 – 800 cm^{-1} are shown in green. Octahedral regions, shown in purple, are responsible for Raman modes from 200 – 500 cm^{-1}. Translational Raman modes from these regions are present at wavenumbers less than 200 cm^{-1}.[3]

7.2.2 Transmission Spectroscopy of β-Ga_2O_3 Films

In order to determine the bandgap value for these films, transmission measurements of a β-Ga_2O_3 film grown on a SiO_2 substrate in the same batch and subjected to the same annealing conditions was performed. The transmission spectrum and the derivative of that spectrum, indicating the bandgap of the material is shown in Figure 7.3. The transmission plot indicates that the annealed films have a bandgap of ~ 4.85 eV which matches the theoretically predicted value for the indirect bandgap of β-Ga_2O_3.[4]

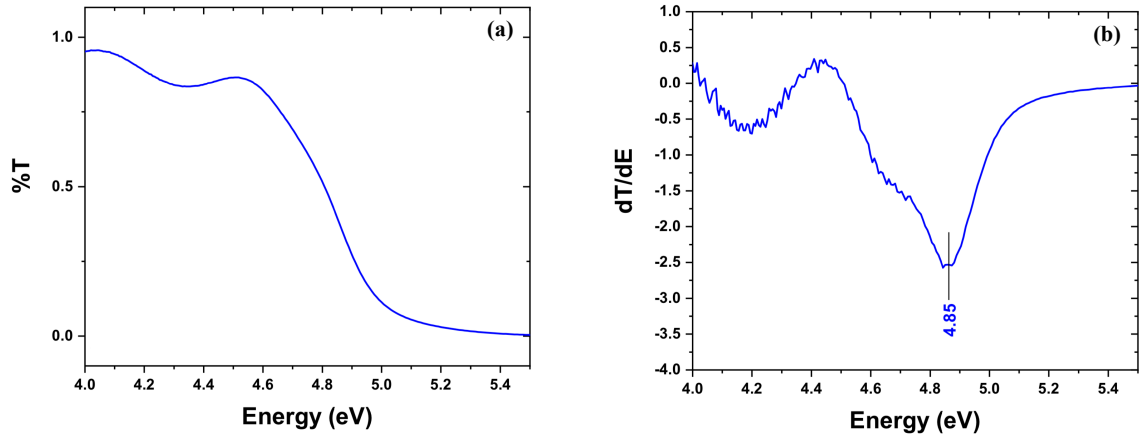

Figure 7.3 (a) Transmission spectrum of β-Ga_2O_3 grown on SiO_2 substrate via RF sputtering. (b) Derivative plot of the spectrum in (a), shows that the bandgap of the β-Ga_2O_3 film is ~ 4.85 eV. The observed value matches the predicted indirect bandgap value for β-Ga_2O_3.

7.2.3 PL Spectroscopy of β-Ga_2O_3 Films

PL spectra of annealed films grown on Si and SiO_2 substrates were collected using micro-PL and above bandgap 5.1 eV (244 nm) laser excitation. Bare substrate spectra were collected and any emissions were subtracted from the film spectra, as done in the Raman spectra. A spectrum for a gallium oxide film grown on Si and annealed in air from sample set 1 is shown in Figure 7.4. This spectrum is similar to all of the PL spectra observed in this sample set on all of the substrates and in all of the annealing environments tested.

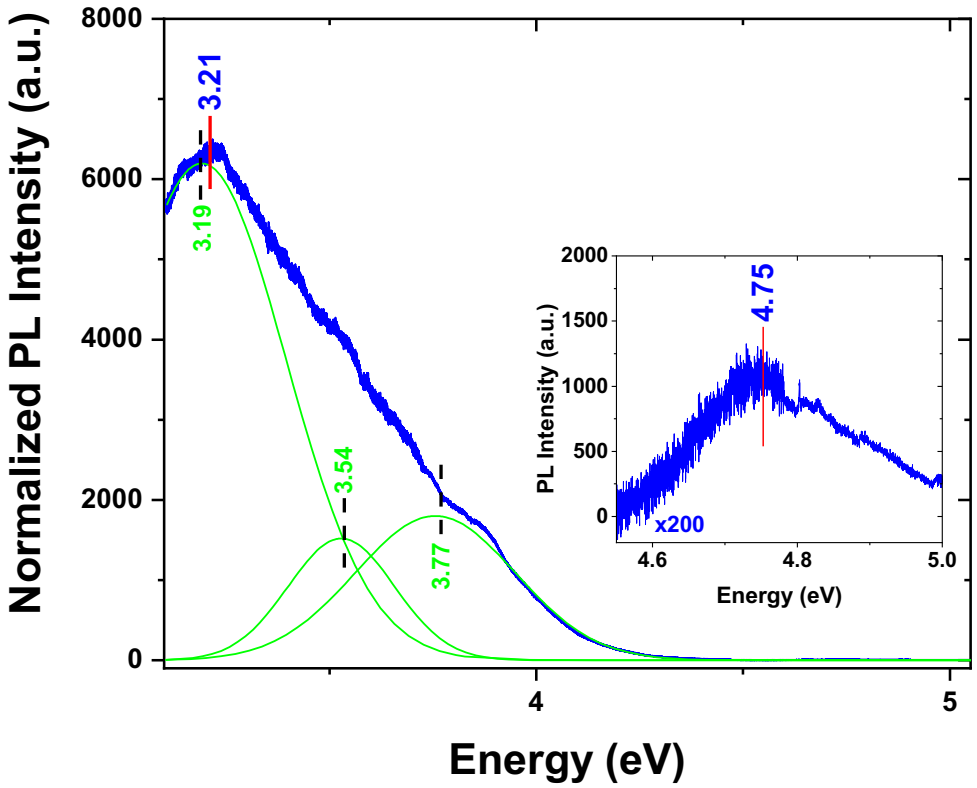

Figure 7.4 PL spectrum of a Ga_2O_3 film on Si <111> grown via RF sputtering in a ~ 2 % oxygen environment. A single broad defect related peak is observed at ~ 3.21 eV, and is typically regarded as a convolution of several PL emissions, shown in green. A weak, deep UV peak at ~ 4.75 eV was also observed, and is shown in the inset, magnified 200x.

The observed PL spectra shown in Figure 7.4 shows a broad PL peak and a weak deep UV peak that is commonly observed. The broad peak is generally considered to be a convolution of several peaks related to self-trapped holes (STH) and crystal defects. The energy value of the observed deep UV peak did not match the band edge value obtained via transmission, and its origin is still being investigated at this time.

During the collection of the PL spectra, an intense blue colored light was emitted from the all of the samples under excitation from the 5.1 eV (244 nm) laser. A Ga_2O_3 film on a SiO_2 substrate under 5.1 eV and 3.8 eV (325 nm) laser excitation is shown in Figure 7.5. The blue emissions have been extensively studied in this material, and are attributed to a defect related donor-acceptor recombination mechanism.[5]

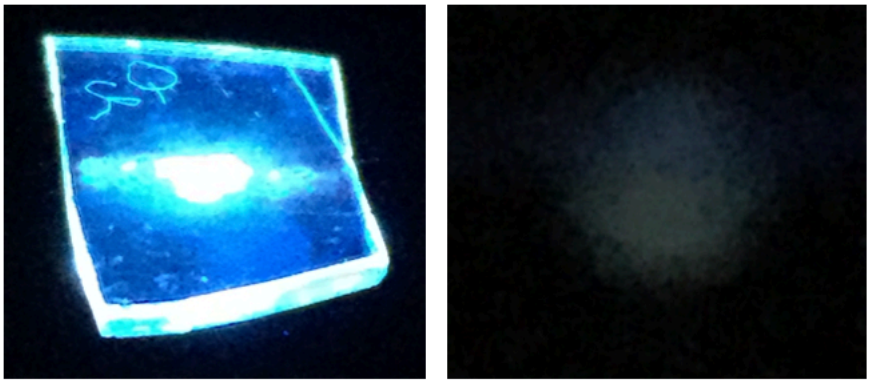

Figure 7.5 Ga_2O_3 film on an SiO_2 substrate under 5.1 eV (244 nm) laser excitation on the left, and the same sample under 3.8eV (325 nm) laser excitation on the right. The blue luminescence is attributed to a defect related donor-acceptor recombination mechanism which is nearly non-existent under 3.8 eV excitation.

The difference in the blue emissions shown in Figure 7.5 along with the PL spectrum shown in Figure 7.4 may provide insight into the mechanism involved. There may be two different donor-acceptor emissions involved in the blue emissions observed, one above 3.8 eV, and another below that energy level that may account for the observed differences. A second mechanism, shown in Figure 7.6, that may be the source of this difference is that a defect level exists at ~ 3.8 eV, allowing the 5.1 eV laser to excite electrons above this level. A large portion of the excited electrons then recombine with an acceptor level, resulting in the intense blue emissions. Excess electrons that do not recombine via the donor-acceptor mechanism would recombine with holes in the valence band, and an associated peak at ~ 3.8 eV would be observed. Evidence of this recombination mechanism is observed via the convoluted peak at 3.77 eV in the spectrum in Figure 7.4.

As shown in Figure 7.7, under 3.8 eV excitation, due to the variation in the energy of the laser light, a small number of photons from the laser are energetic enough to excite electrons in the material to the ~ 3.8 eV defect energy level. This small number of electrons could then recombine via the same mechanism previously mentioned, resulting in the faint blue emissions observed in Figure 7.5. Since the ~3.8 eV level is close to the energy of the laser, PL measurements using the 3.8 eV laser cannot be performed. Verification of the existence of the ~ 3.8 eV peak during sub-bandgap excitation at ~ 4 eV is required to advance work on this mechanism, and may be the subject of future work.

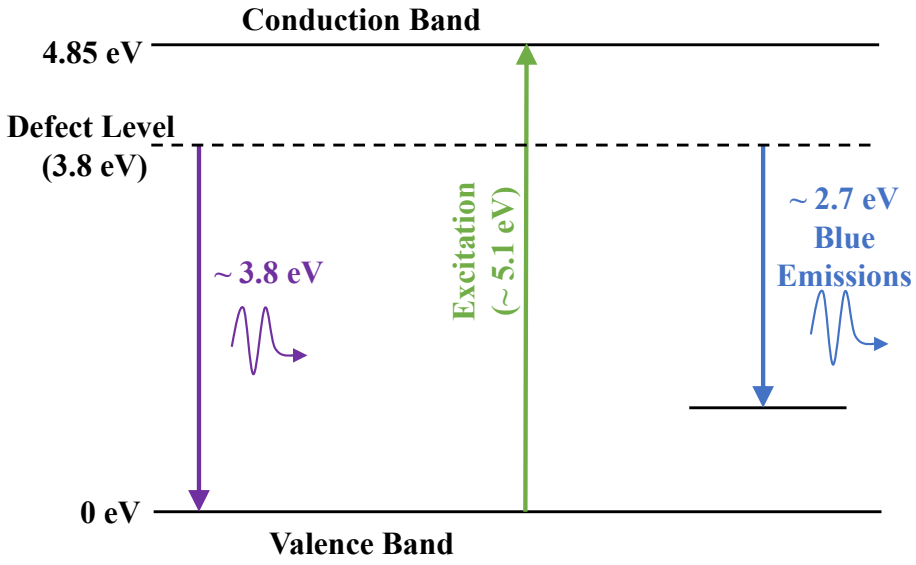

Figure 7.6 Excitation of the film with above band gap excitation results in intense visible blue emissions, shown in Figure 7.5, from a donor-acceptor recombination mechanism. A weak UV-PL emission is also present at ~ 3.8 eV, shown in the convoluted PL spectra in Figure 7.4.

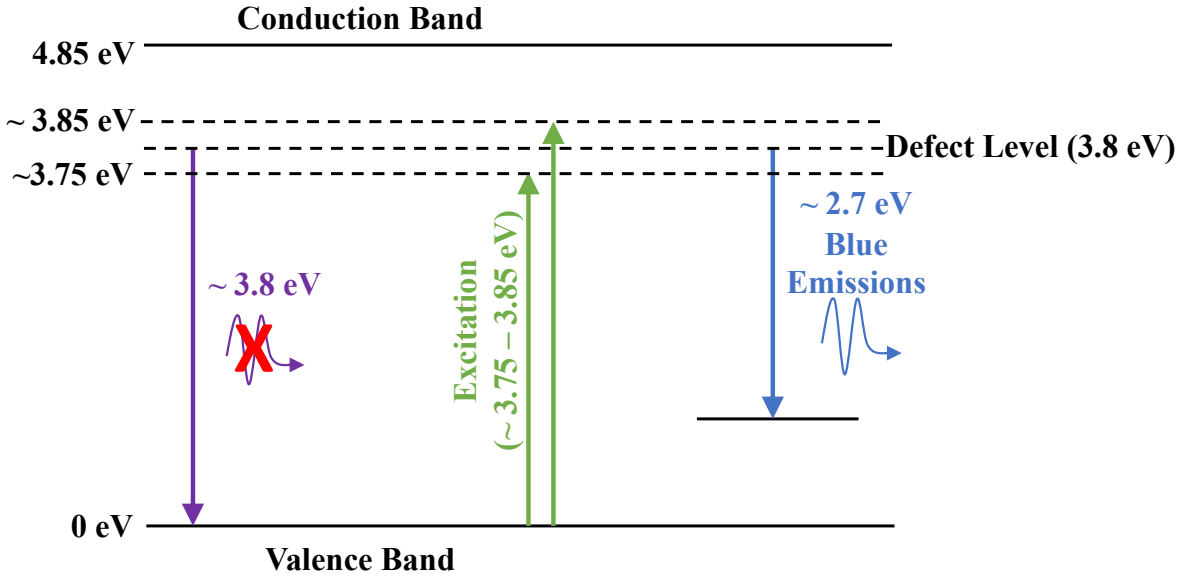

Figure 7.7 Excitation of the film with sub-band gap excitation of ~ 3.8 eV results in weak blue emission, shown in Figure 7.5, from a donor-acceptor recombination mechanism. The difference in the intensity of the emissions, and the PL spectra of the film under ~ 5.1 eV excitation, suggests a defect level exists at ~3.8 eV. Defect level to conduction band emissions were not observed with ~ 3.8 eV excitation, since the detector is saturated by the laser light at this energy.

Due to the results of the previous experiments, an attempt to improve the film growth parameters was undertaken. Specifically, the strong blue emissions observed and the presence of the broad ~ 3.21 eV peak in the PL spectrum indicated that the films had a high density of defects that should be addressed with a new growth. Additionally, the mismatch between the deep UV peak in the PL spectrum and the theoretically predicted band edge value that was also observed via transmission was considered when selecting growth parameters for the second sample set. In response to these considerations, the deposition time, deposition power, and oxygen concentration in the growth environment were changed.

7.3 Revised Growth Method for β-Ga_2O_3 Films

In order to improve the Ga_2O_3 films, a second set of films were grown (see Table 7.1) that resulted in thinner films. The rationale behind changing the power and deposition time was that a thinner film would still allow for characterization of the films, while the higher power and shorter deposition time was expected to reduce wear on the sputtering system and lengthen the target life. The change in oxygen content was based on literature that indicates that β-Ga_2O_3 has a sensitivity to oxygen in the growth environment. This previous work also indicated that sputtered films require a growth environment of 1% to 5% oxygen in order to be suitable for optical characterization.[6] In studies that utilized annealing, the effects of an oxygen-rich or oxygen-poor growth environment could not be overcome via post-deposition annealing.[6] The reason for this is that in an oxygen-poor environment Ga_2O_3 gives oxygen up to the sputtering environment, while an oxygen-rich environment results in excess oxygen deposition in the films. Both result in nonstoichiometric films that will exhibit traits of defects such as oxygen vacancies and interstitials, and gallium interstitials.[7] Within the 1% to 5% range of oxygen concentration there can still be nonstoichiometric film deposition, so for the second growth, the oxygen content in the growth environment was reduced from ~ 2% to ~ 1.4% in an attempt to grow higher quality films.

7.3.1 Transmission Spectroscopy of β-Ga_2O_3 Films

Transmission spectroscopy was once again used for the lower oxygen growth samples to determine the bandgap of the materials. The films grown as part of sample set 2 were grown according to the previously mentioned parameters, with the significant changes listed

in Table 7.1. Since the changes to the growth parameters were small, the results were expected to be similar, with the greatest change in transmission being the thickness of the samples. The transmission spectra revealed that the post-annealed sample thickness of the films was ~ 350 nm. The transmission spectrum and resultant derivative plot are shown in Figure 7.8. The transmission spectrum was consistent with the expected result, revealing a bandgap value of 4.85 eV, so further analysis of this set of films continued with PL analysis.

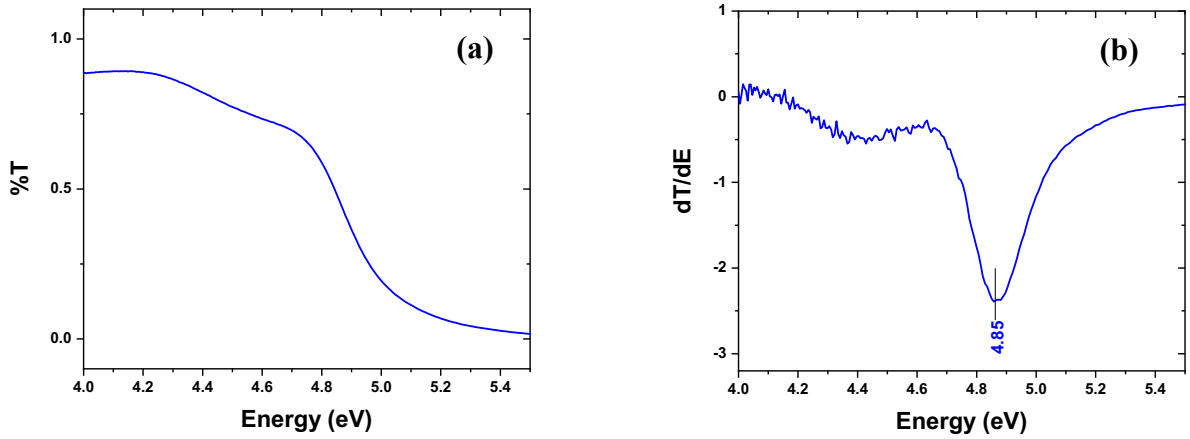

Figure 7.8 (a) Transmission spectrum of a Ga_2O_3 film on a SiO_2 substrate, post-annealing, and (b) the resulting derivative spectra showing that the bandgap of the film is ~ 4.85 eV. As expected, this value is consistent with the measured bandgap of the previous sample set grown in a ~ 2% oxygen environment.

7.3.2 PL Spectroscopy of β-Ga_2O_3 Films

The initial PL analysis of the annealed β-Ga_2O_3 films grown in a ~ 1.4% O_2 environment was performed with ~ 32.5 mW, 5.1 eV (244 nm) above bandgap excitation. Upon placing the first sample in the laser path, the bright blue emissions observed in the previous sample set grown in ~ 2% O_2 was absent, and was replaced with a faint red emission. A photo of β-Ga_2O_3 films grown on SiO_2 substrates in ~ 2% and ~ 1.4% O_2 environments is shown in Figure 7.9. This initial observation suggested that the quality of the samples grown in a ~ 1.4% O_2 environment was higher than the samples grown in ~ 2% O_2. Following this observation, a PL spectrum, shown in Figure 7.10, of a Ga_2O_3 film that was air-annealed for 3 hours at 1100º C was obtained.

Figure 7.9 Two Ga_2O_3 films on SiO_2 substrates under 5.1 eV laser excitation. The film on the left was grown in a ~ 2% oxygen environment, and displays intense blue emissions characteristic of defect related emissions. The sample on the right was grown in a ~ 1.4% oxygen environment, and does not exhibit the same donor-acceptor defect related emissions. The samples were positioned to receive approximately the same amount of laser light for this observation.

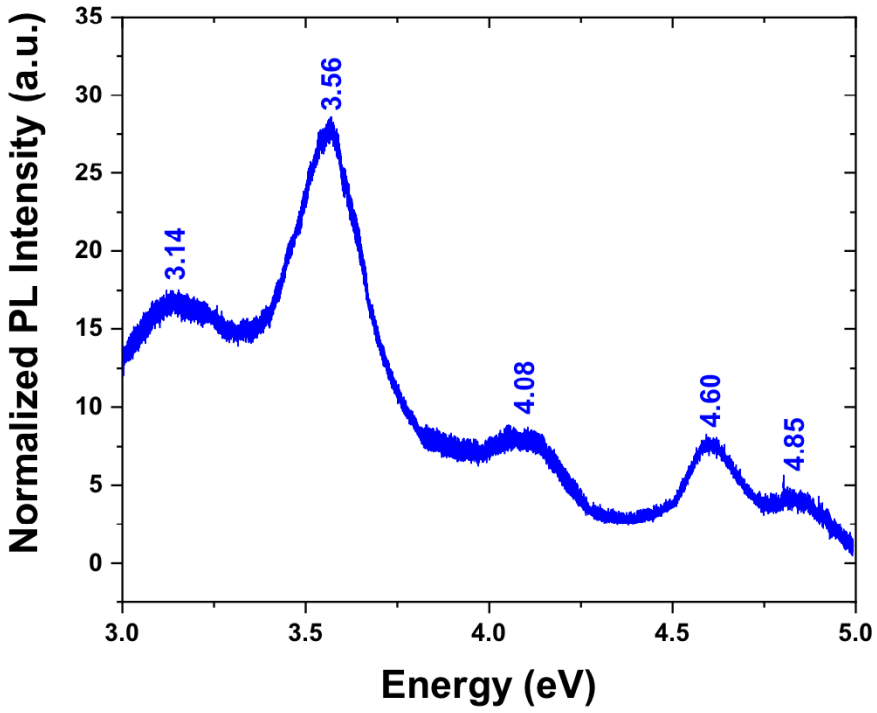

Figure 7.10 PL spectrum of Ga_2O_3 on a Si substrate, grown via RF sputtering. Reduction of the oxygen concentration in the growth environment produced higher quality films and a resolved spectra was obtained.

The PL spectrum shown in Figure 7.10 verifies the initial assumption from the visual observation in Figure 7.9, that by changing the oxygen concentration in the growth environment by ~ 0.6%, a significant change in the quality of the films was obtained. The spectrum reveals five distinct peaks in the UV region of the electromagnetic spectrum, with weak, broad, deep UV emissions at the predicted band edge value of ~ 4.85 eV.[4] This band edge value is consistent with the value from the derivative analysis of the transmission spectrum shown in Figure 7.8(b).

The lack of blue emissions in the sample grown in the ~ 1.4% oxygen environment and the low intensity of the ~ 3.14 eV peak in Figure 7.10, reinforces the idea that the defect related mechanism for the blue emissions was nearly eliminated. It is likely that elimination of this defect mechanism allowed more electrons and holes to remain in the conduction band and valence band, respectively, increasing the band edge recombination rate. Studies of the visible and near-UV properties of this material have been extensively researched, and since visible emissions was not the focus of this research, additional research was not performed on the origin of the blue emission mechanism.[8-10]

In response to obtaining a resolved spectra, an experiment was performed to try to determine which of the peaks observed in Figure 7.10 are associated with self-trapped holes (STH), which were discussed in Chapter 1.5. The sample used to obtain the spectra in Figure 7.10 was subsequently excited with a 3.8 eV laser. Sub-bandgap excitation should eliminate the self-trapped hole mechanism since hole creation would not be expected if the electron is not excited to the conduction band. The result of this experiment is shown in Figure 7.11, and schematically explained in Figure 7.12.

The lack of a peak in the ~ 3.56 eV region under 3.8 eV excitation shows that the ~ 3.56 eV peak observed with 5.1 eV excitation is associated with the self-trapped holes. The high intensity of this peak, coupled with the weak band edge emission at ~ 4.85 eV, indicate that this material is unlikely to be an efficient band edge emitter. The ~ 3.14 eV peak associated with the donor–acceptor mechanism behaved exactly as expected based on the previous observations discussed in Chapter 7.2.3.

The existence of the strong STH mechanism in β-Ga_2O_3 that produces the strong peak at ~ 3.56 eV was expected to completely quench the bandgap PL emissions from this material. Although weak bandgap emissions were observed in our films, the strong STH

mechanism still severely limited the number of holes in the valence band available for recombination across the bandgap. Since the STH emissions are due to an intrinsic property of the material, and are not a typical defect related sub-bandgap emission, improving the crystal structure of the material via typical treatment methods such as annealing or coating is not expected to improve the bandgap emission intensity relative to the STH emissions.

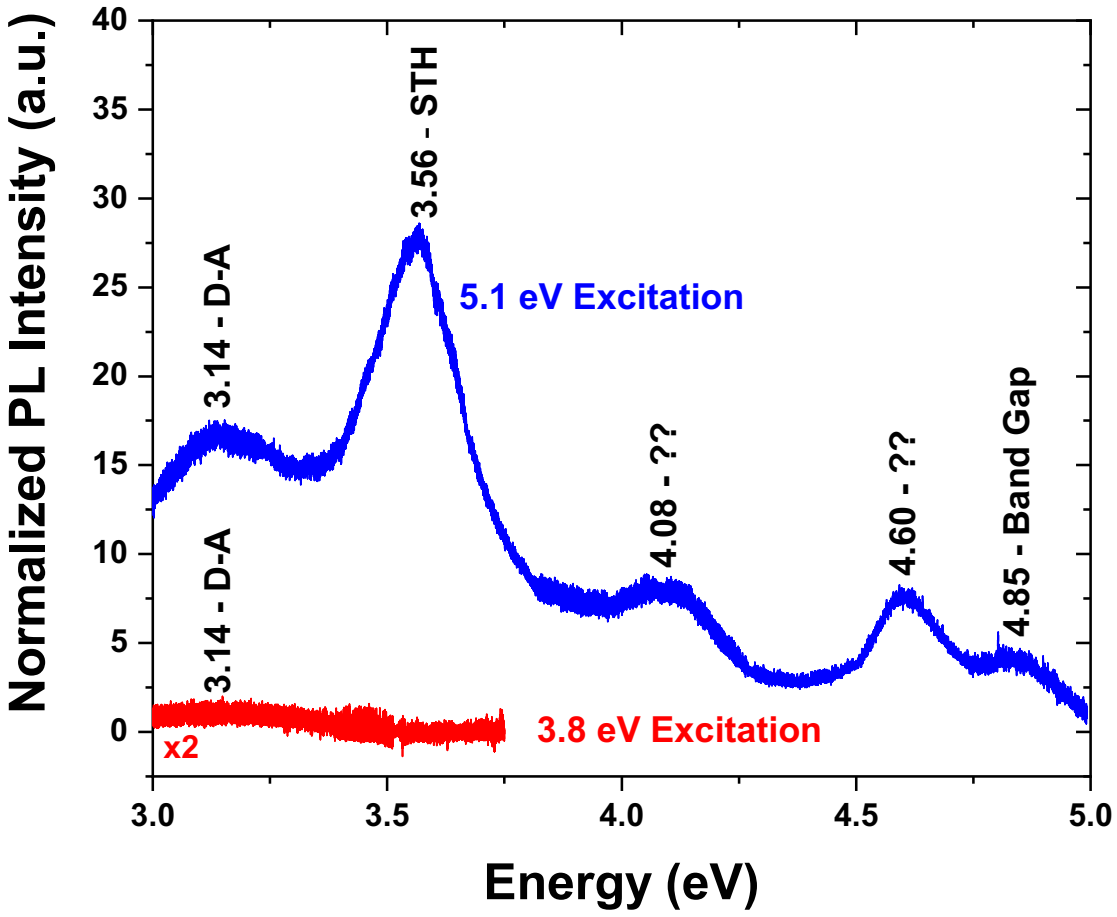

Figure 7.11 PL spectra of a Ga_2O_3 film on an Si <111> substrate excited with an above bandgap 5.1 eV (244 nm) laser (blue), and a sub-band gap 3.8 eV (325 nm) laser (red). The absence of a peak at ~ 3.56 eV in the sub-bandgap 3.8 eV excitation spectrum indicates that this peak is likely associated with self-trapped holes.

As a result of the information obtained thus far about the PL spectra, a band diagram showing the transitions for these peaks is shown in Figure 7.12. The mechanisms responsible for the peaks at ~ 4.08 eV and ~ 4.60 eV have not been identified, but will be further discussed further in Chapter 8.

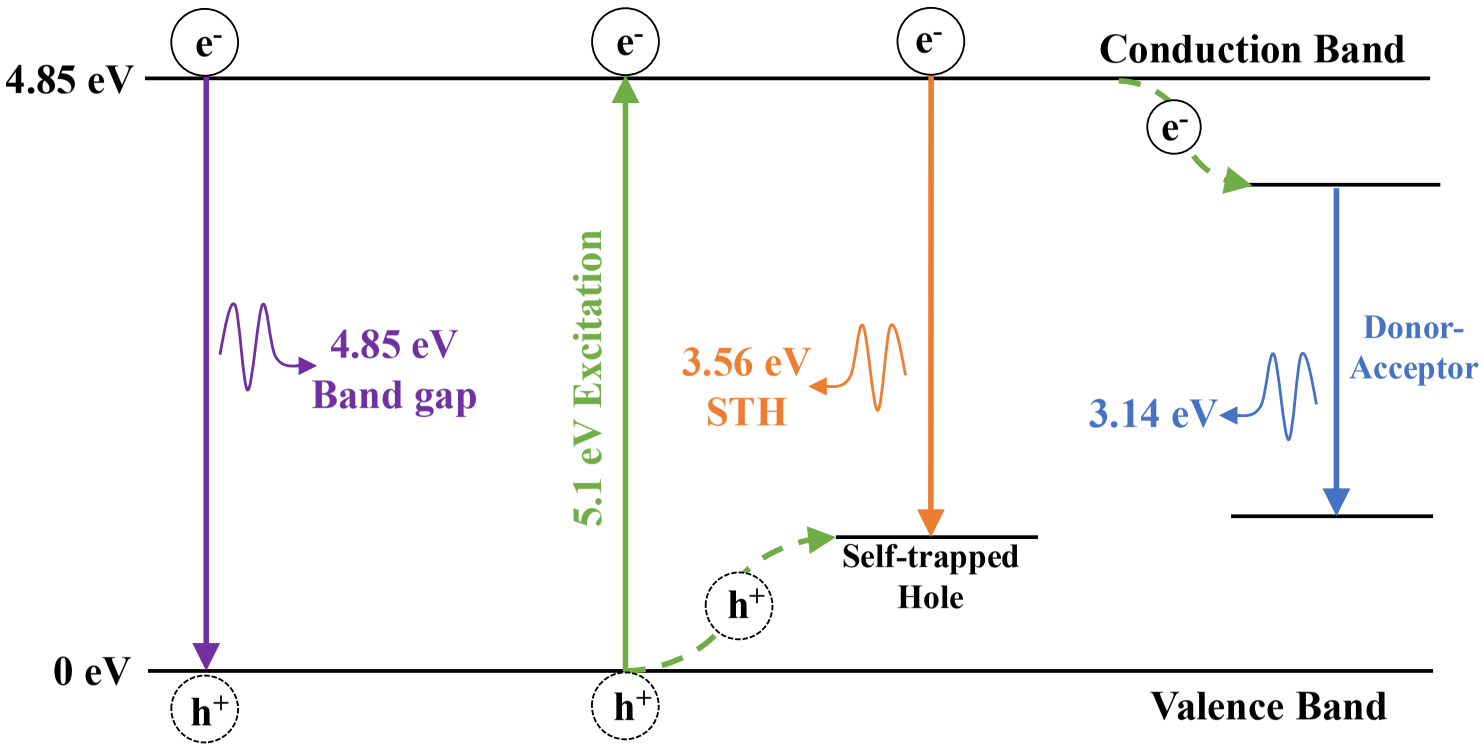

Figure 7.12 Band diagram showing transition mechanisms for various peak emissions with above bandgap excitation. Holes created by the elevation of the electron to the conduction band are trapped at a higher energy level, resulting in the ~ 3.56 eV peak. Crystal defects and impurities create energy levels inside of the badgap that can lead to electron-hole recombination, which produces the peak at ~ 3.14 eV. A small fraction of the electron-hole pairs complete a conduction band to valence band recombination that results in the ~ 4.85 eV band edge emission. With sub-band gap excitation (3.8 eV laser), free electron-hole pairs are not created, therefore the route to STH is eliminated, resulting in no PL.

7.3.3 Structure and Composition of β-Ga_2O_3 Films

Raman spectra from the samples grown in a ~ 1.4% O_2 environment were similar to the spectrum shown in Figure 7.1, implying that this sample has the β-phase. For this set of films, additional characterization was performed using SEM and EDS to provide additional information about their structure and composition. An image of an annealed Ga_2O_3 film grown on a Si <111> substrate were taken using the in-lens detector, and are shown in Figure 7.13.

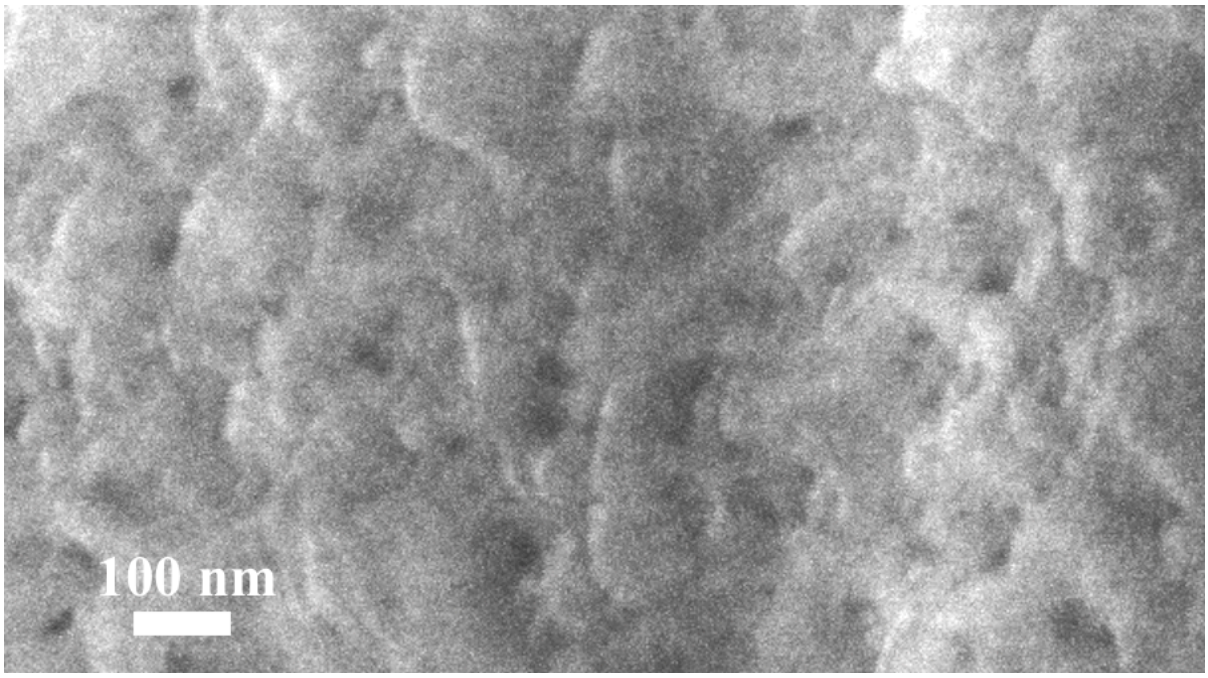

Figure 7.13 SEM image of an annealed Ga_2O_3 film grown in a ~ 1.4% O_2 environment taken at 30kx magnification using an in-lens detector.

The SEM image shown in Figure 7.13 shows that the morphology of the film is relatively smooth, with the coalescence of grains. Finally, an EDS analysis of the film in Figure 7.13 was performed to determine the composition of the film. The EDS analysis showed that the films are ~ 2 % O_2 deficient by mass, and ~ 3% O_2 deficient by atomic ratio. This is expected after annealing in air, as annealing is expected to result in a net loss of oxygen from the films, similar to the oxygen loss previously noted during growth. However, the results of the EDS analysis, shown in Figure 7.14, show that the films remained within the margin of error for the expected 2:3, Ga:O ratio.

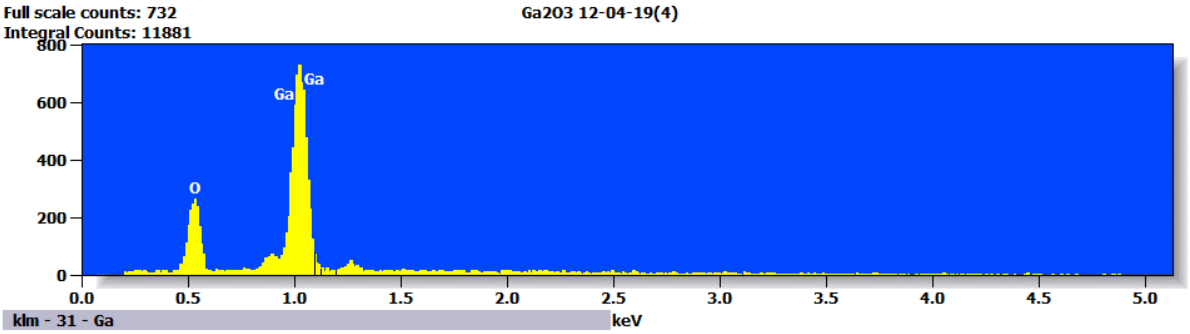

Element	*Net Counts*	*Net Counts Error*	*K-Ratio*	*ZAF*	*Weight %*	*Weight % Error*	*Atom %*	*Atom % Error*
O	1691	± 98	0.3	1.03	23.6	± 0.7	57.4	± 3.3
Ga	3429	± 180	0.7	1.15	76.4	± 2.0	42.6	± 2.2
Total					100.0		100.0	

Figure 7.14 EDS data from an air-annealed β-Ga_2O_3 film. The films were slightly oxygen deficient, but within the margin of error for the EDS detector. Any oxygen deficiency that exists is likely due to air-annealing, which increases the likelihood of oxygen loss from the films.

This EDS information indicates that the oxygen content in the growth environment is nearly ideal to achieve stoichiometric films. Further EDS analysis of the films grown in a ~ 2% environment, and a complete annealing study of these films is required to determine the optimal environment for growth and annealing. In response to this data, an preliminary annealing study of the effects of annealing environments was performed.

7.3.4 Effects of Annealing Environment

It is well established that metal-oxide semiconductors are prone to oxygen interactions. In order to gain some insight into the issue, two samples were annealed in different oxygen environments: one in air (~ 20% O_2 content), and another in an environment with > 95% O_2 content. The annealing temperature was maintained 1100º C for 3 hours. One set of samples was annealed in O_2, and the other in air. The PL spectra of the films are presented in Figure 7.15.

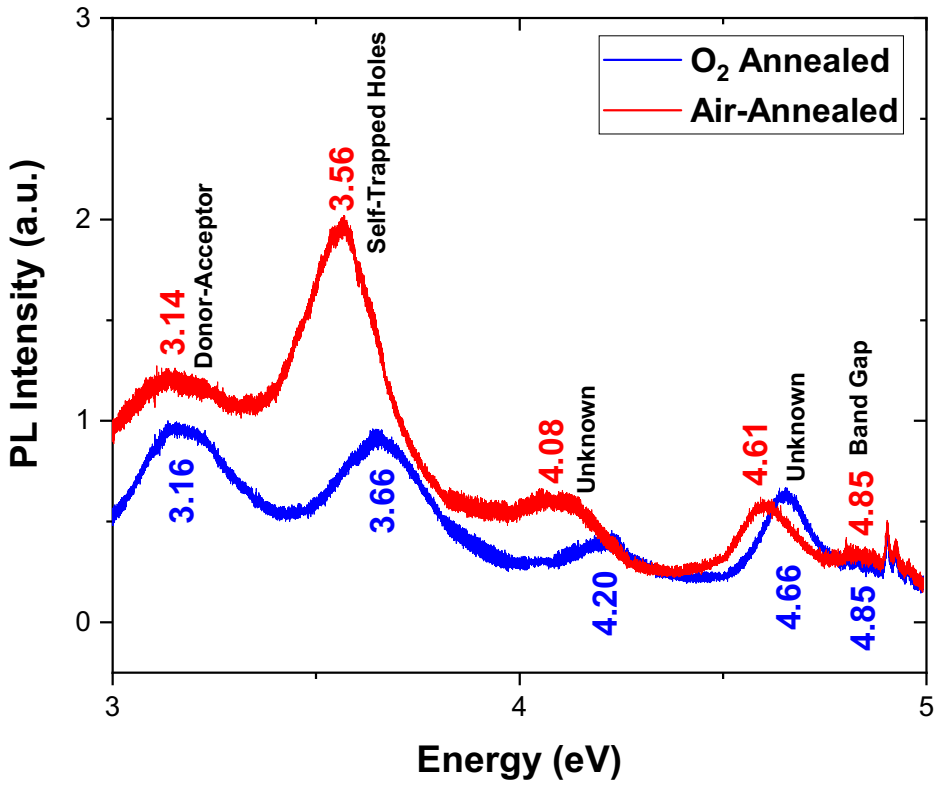

Figure 7.15 PL spectra of β-Ga_2O_3 films, annealed in air (red), and O_2 (blue) under ~ 32.5 mW, 5.1 eV above bandgap laser excitation. A significant blue shift of the peaks after annealing in oxygen was observed. Annealing in oxygen also reduced the STH intensity and increased the relative defect-related intensity. A similar band edge intensity was measured for samples from both annealing environments.

As can be seen in the figure, annealing in oxygen has a strong impact on the optical properties. Two main observations are: the unknown PL emission at 4.08 eV blue shifted to 4.20 eV, which is considered to be a meaningful shift (~ 120 meV), moreover, the intensity of the emissions from STH decreased significantly. Presently it can be suggested that the unknown peak at 4.08 eV is related to emissions originating from oxygen-complex type defects. Usually such dramatic PL shifts can be attributed to a change in the energy levels of the defect center. Deep-level defects can create a band in the band gap, thus higher concentrations of defects will result in a wider band that results in a higher energy emission. Additionally, the reduction of the STH can tentatively be attributed to weakening of the electrostatic field that traps the holes to the oxygen in Ga_2O_3. Future work will address this topic.

7.4 Summary

Initial research on air annealed, RF sputtered β-Ga_2O_3 thin films was performed. Raman, PL, and transmission spectroscopy were used to study the optical properties of this material. The composition of the films was studied via EDS, and SEM was used for imaging of the film surface. The primary results of this research are:

- As determined via Raman spectroscopy, the sputtered films in this study form the monoclinic β-Ga_2O_3 crystal structure after annealing at 1100º C.
- Transmission spectra of the annealed, sputtered films consistently exhibit a band edge value of ~ 4.85 eV, which is in agreement with theoretical values commonly found in literature.[4]
- PL spectra of films grown in an environment of ~ 2% oxygen and ~ 98% argon exhibit a commonly observed broad, convolved, intense peak at ~ 3.21 eV, along with a weak deep-UV peak at ~ 4.75 eV.
- Films grown in a ~ 1.4% oxygen and ~ 98.6% argon environment produce a PL spectrum with five distinct peaks in the UV range of the electromagnetic spectrum.
- Weak PL band edge emissions of ~ 4.85 eV are observed in the films grown in a 1.4% oxygen environment. This band edge value was confirmed via transmission spectroscopy, and is in agreement with theoretical work.[4]
- A combination of sub-bandgap and above bandgap excitation was used to identify self-trapped holes as the origin of an observed peak at ~ 3.56 eV. This value is similar to theoretically predicted values from literature.[11]
- A band diagram for three of the UV peaks was developed. Peaks observed at ~ 4.08 eV and ~ 4.60 eV remain unidentified.
- EDS indicated that the composition of the films grown in a ~ 1.4% oxygen environment is nearly stoichiometric.
- Defects in films grown in higher oxygen concentrations are more prevalent due to excess oxygen, likely leading to oxygen interstitials.
- Annealing the films in an oxygen environment yields a blue shifted PL spectrum for three of the UV peaks. The band edge and donor-acceptor PL emissions remain constant for air-annealed and O_2-annealed films.

7.5 References

1. L.B. Freund and S. Suresh, *Thin Films Materials:Stress, Defect Formation and Surface Evolution*, (Cambridge University Press, New York, 2003) pp 2–5.
2. D. Dohy, G. Lucazeau, and A. Revcolevschi, J. Solid State Chem., **45**, 180 (1982).
3. H. Peelaers, H. and C.G. Van de Walle, Phys. Status Solidi B **252**, 828 (2015).
4. C. Janowitz, V. Scherer, M. Mohamed, A. Krapf, H. Dwelk, R. Manzke, Z. Galazka, R. Uecker, K. Irmscher, R. Fornari, M. Michling, D. Schmeißer, J.R. Weber, J.B. Varley, and C.G.V. de Walle, New J. Phys. **13**, 085014 (2011).
5. T. Onuma, Y. Nakata, et al. "Modeling and interpretation of UV and blue luminescence intensity in β-Ga_2O_3 by silicon and nitrogen doping", J. Appl. Phys. **124**, 075103 (2018).
6. A.K. Saikumar, S.D. Nehate, and K.B. Sundaram, ECS J. Solid State Sci Technol. **8**, Q3064 (2019).
7. S. Li, S. Jiao, D. Wang, S. Gao, and J. Wang, Journal of Alloys and Compounds **753**, 186 (2018).
8. L. Binet and D. Gourier, J. Phys. Chem. Solids **59**, 1241 (1998).
9. E.G. Villora, M. Yamaga, T. Inoue, S. Yabashi, Y. Masui, T. Sugawara, and T. Fukuda, Jpn. J. Appl. Phys. **41**, 6 (2002).
10. T. Onuma, Y. Nakata, K. Sasaki, and T. Masui, J. Appl. Phys. **124**, 075103 (2018).
11. S. Yamaoka, Y. Furukawa, and M. Nakayama, Phys. Rev. B **95**, 094304 (2017).

Chapter 8: Conclusion

8.1 ZnO Thin Film UV-PL Intensity Enhancement

Optical coatings of Al_2O_3, SiO_2 and MgO were utilized in this research to successfully enhance the UV-PL intensity of ZnO thin films via passivation of surface defects. MgO coatings were found to provide the greatest intensity improvement by enhancing the UV-PL by 52 times over an annealed uncoated ZnO film. Additionally, a strong linear correlation between the UV-PL intensity improvement of the films and the average intra-molecular bond energy of the coating material was observed.

It was also determined that annealing of the ZnO films before coating deposition was required to achieve the greatest UV-PL intensity improvement, with a 900º C annealing temperature producing greatest intensity improvement by the coating. A separate annealing study revealed that this annealing step removes defects from the subsurface bulk of the film. Deposition of the coating then addressed the surface defects such as OH-groups not addressed by annealing.

Additionally, annealing after coating deposition caused the PL intensity to diminish with respect to as-grown coatings. Annealing disturbed the bonds at the coating-ZnO interface, allowing non-radiative centers to return to the ZnO surface, resulting in lower UV-PL intensity. Future work includes the use of different coating and luminescent materials, which can be used to verify the relation between the PL intensity improvement and the average coating bond energy that was observed in this research. Additional adjustments to the growth and annealing process may also improve the performance of these coatings and provide additional insight into the mechanisms responsible for the UV-PL intensity improvements observed in this work.

Finally, one drawback to using MgO as a coating material is that it is subject to degradation when exposed to air. Over time, environmental exposure caused a compositional change in the MgO coating, which resulted in the lower UV-PL intensity observed at the end of the 294-day experimental period.

8.2 β-Ga_2O_3 Thin Film Optical Properties

Ga_2O_3 thin films were grown via RF sputtering on Si and SiO_2 substrates. The films were subjected to two different growth environments. One set of films was grown in an Ar:O_2 environment with a ~ 2% O_2 concentration, while the other set was grown in an adjusted environment with a ~ 1.4% O_2 concentration. Post-deposition air-annealing was performed on the samples to improve the quality of the polycrystalline films. Raman, PL and transmission spectroscopy were used to obtain initial optical characteristics of these films, and EDS was used to determine the composition of the films.

As expected, Raman spectroscopy revealed that the annealed films were monoclinic β-Ga_2O_3. The Raman spectra were similar, regardless of the O_2 concentration in the growth environment. Transmission measurements of the annealed β-Ga_2O_3 films grown on SiO_2 provided a band edge value of ~ 4.85 eV for both sets of films. This is also the theoretically predicted value for β-Ga_2O_3.

PL spectra of annealed β-Ga_2O_3 films grown in a ~ 2% O_2 growth environment on Si <111> substrates displayed a commonly observed, broad defect related peak at ~ 3.21 eV, and a weak, sub-bandgap deep UV peak at ~ 4.75 eV. The broad peak at ~ 3.21 eV is typically considered a convolution of multiple PL peaks, and minor shoulders in the observed peak indicate that this is likely the case. In this research, the room temperature intensity of this peak is ~ 300 times more intense than the ~ 4.75 eV peak. Intense blue emissions, from donor–acceptor recombination events, were observed in samples from this growth as well.

The goal of the second growth was to increase the sample quality by reducing the oxygen content in the growth environment, which would result in a more stoichiometrically correct film composition. These films, grown in a ~ 1.4% O_2 environment, produced a PL spectra with five distinct peaks, including weak band edge emissions at ~ 4.85 eV. The resolved spectra, the lower intensity of the defect related peak, along with the blue emissions being extinguished, indicates that the quality of the film improved in the ~ 1.4% growth environment. Subsequent EDS analysis showed that the films were slightly oxygen deficient, but stoichiometrically correct within the equipment tolerance. It is believed that in an oxygen-rich growth environment, significant concentrations of defects, such as oxygen interstitials, provide a highly favorable recombination mechanism that produces the intense sub-bandgap emissions.

Additional PL analysis of the air-annealed samples using sub-bandgap excitation provided evidence that emissions due to self-trapped holes (STH) is centered at ~ 3.56 eV, which also agrees with theoretically predicted values from literature. Since the STH is not a defect, but a property that is intrinsic to this material, it is a factor that limits the ability of this material to be an efficient band edge emitter. An annealing study that focused on the effects of changes in the oxygen concentration in the annealing environment showed that the PL spectrum blue shifts significantly as the oxygen content rises. This study shows that β-Ga_2O_3 is an ideal material for use in high temperature oxygen sensing devices.

8.3 Future Work

8.3.1 ZnO Coatings

The following items are topics of interest that may be the subject of future work on coatings as a means of enhancing the PL intensity of luminescent materials:

- Research of additional coating materials such as CaO or ZrO_2 may be useful to extend this research.
- A study on limiting the impact of environmental degradation of the MgO coatings is required to realize the full potential of this coating material in device technologies.
- A preliminary PL study of a MgO coated $Mg_{0.2}Zn_{0.8}O$ film was performed that showed a similar, but significantly less effective enhancement of the UV-PL intensity. This result is shown in Figure 9.1. A future study may provide a method for applying coatings that realizes a greater intensity improvement on these alloyed films that typically possess a much lower PL intensity than that of the ZnO films.
- Identification of the source of the MgO coating degradation after an environmental exposure will provide information that may be useful to mitigate the coating degradation, and realize the full potential of the MgO coating in devices.

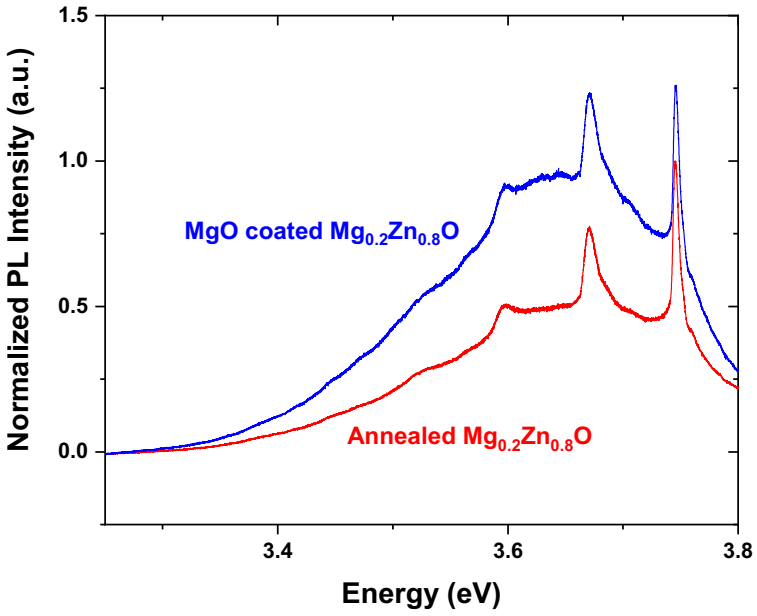

Figure 8.1 PL spectra of $Mg_{0.2}Zn_{0.8}O$ films before and after coating with MgO. UV-PL intensity improvements observed by coating these films followed similar trends observed in ZnO films, but the enhancements were significantly less than with the ZnO films. Additional work is required to optimize the coating process for this alloy.

8.3.2 Ga_2O_3 Thin Films

The following items are topics of interest that may be the subject of future work on Ga_2O_3 thin films:

- Additional studies to determine the origin of the observed emissions at ~ 4.08 eV and ~ 4.60 eV.
- Further research into the defect level that exists at ~ 3.8 eV, including additional understanding of the mechanism that is responsible for the UV and visible blue emissions that are associated with this defect.
- Temperature dependent PL, Raman and transmission studies of the Ga_2O_3 films to provide additional information about the mechanisms behind the observed emissions. These studies may also provide insight into the unidentified emissions previously mentioned in this section.